CFP fluorescence emission ratios), which reflect ATP levels in living cells, were calculated from the fluorescent images of CFP and Venus, a variant of YFP that is resistant to intracellular pH [18], within the cytoplasm of individual cells. Each independent measurement was plotted as indicated in Figure 2. Uniform Venus/CFP ratios were observed in Huh-7 cells. These ratios were reduced dramatically following combined treatment with 2-deoxyglucose (2DG) and Oligomycin A (OliA), which inhibit glycolysis and the oxidative phosphorylation of ADP to ATP, respectively [2]. When AT1.03^{YEMK} was expressed in the HCV replicon-harboring cells JFH-1/4-1, JFH-1/4-5 (genotype 2a) and NK5.1/0-9 (genotype 1b) [15], Venus/CFP ratios were significantly lower than those seen in parental Huh-7 cells. This result is consistent with the mass spectrometry results shown in Figures 1A and S1. Venus/CFP ratios were more variable in the replicon-carrying cells compared to Huh-7 cells. It is possible that ATP levels in the replicon cells correlate with viral replication levels, which may vary among the cells tested.

The consumption of ATP is increased in HCV-replicating cells

It has been reported that ATP is involved in different steps in the course of HCV replication such as in the initiation of RNA synthesis by NS5B RdRp [9]. NS3 unwinds RNA in an ATP-dependent manner and may be involved in viral replication [11,19,20]. NS4A has been shown to enhance the ability of the NS3 helicase to bind RNA in the presence of ATP [21]. In addition, ATP is generally used as a material in RNA synthesis. Together with the above results (Figures 1 and 2), one may hypothesize that active consumption of ATP in cells where HCV RNA replicates efficiently results in lower levels of cytoplasmic ATP compared to cells in the absence of the viral RNA. To study the influence of HCV RNA replication on the consumption of ATP in cells, we used permeabilized HCV replicon cells [13,22].

Following the addition of ATP to permeabilized cells, reduced ATP levels were detected using a luciferase-based assay (see Materials and Methods for details). Fifteen minutes after the addition of ATP, ATP levels in permeabilized replicon-carrying cells (JFH-1/4-1, JFH-1/4-5 and NK5.1/0-9) were reduced by 82–95%, and this reduction was greater than that observed in control Huh-7 cells (47%)(Figure 3). When the replication of HCV RNA was inhibited by pre-treatment of the cells with the cytidine analogue inhibitor of HCV NS5B polymerase, PSI-6130 [23,24], for 3 days, the reduction in ATP levels in the replicon cells was comparable to that of Huh-7 cells. A decrease in ATP reduction in the replicon cells was observed even following a 15-min treatment with the inhibitor. An effect of inhibition of viral replication on cytoplasmic ATP levels in replicon cells was also observed by ATeam-based analysis of Venus/CFP ratios following inhibition of replication by IFN-alpha (Figure S2). These results suggest that ATP is actively consumed during viral replication in HCV replicon cells, leading to decreased levels of ATP in the cytoplasm.

Development of a system to monitor ATP levels at putative subcellular sites of HCV replication in single living cells

Moradpour et al. have established functional HCV replicons that have either an epitope tag or the coding sequence for a green fluorescent protein (GFP) inserted in frame close to the C-terminus of NS5A, which they used to demonstrate incorporation of the NS5A-GFP fusion protein into the viral RC [25]. To further investigate intracellular changes in ATP during HCV replication, we generated HCV JFH-1-based subgenomic replicons harboring an ATeam insertion in the 3′ region of NS5A (SGR-ATeam), as

	No. cells	Venus/CFP ratio mean	Venus/CFP ratio SD	p-value vs Huh-7
Huh-7	19	2.08	0.090	
Huh-7 + 2DG, OliA	13	0.66	0.074	$< 1x10^{-29}$
JFH-1/4-1	18	1.79	0.14	$< 1x10^{-7}$
JFH-1/4-5	18	1.77	0.28	0.00019
NK5.1/0-9	19	1.66	0.30	$< 1x10^{-5}$

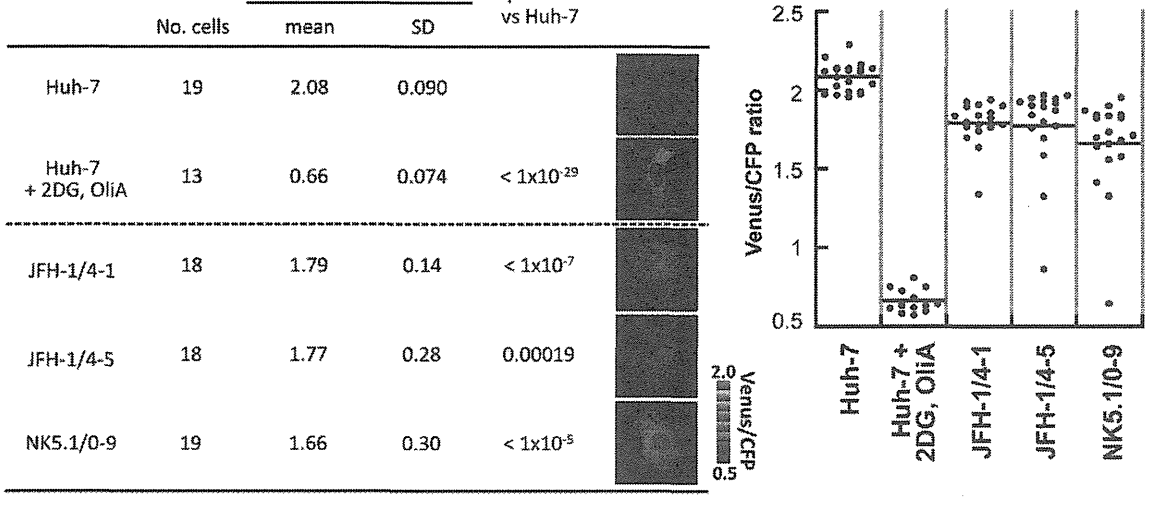

Figure 2. ATP fluctuations within the cytoplasm of HCV replicating cells analyzed using the original ATeam. Huh-7 cells carrying a HCV subgenomic replicon, JFH-1/4-1, JFH-1/4-5 (genotype 2a), and NK5.1/0-9 (genotype 1b) and parental Huh-7 cells were transfected with an ATP probe, AT1.03^{YEMK}. Forty-eight hours after transfection, the Venus/CFP emission ratio in the cytoplasm of each cell was calculated from fluorescent images acquired with a confocal microscope FV1000 (Olympus). Huh-7 cells treated with 10 mM 2-DG and 10 μg/ml OliA for 20 min were used as a negative control. Data are presented as means and standard deviation values (SD) for each cell. Statistical differences among Huh-7 cells were evaluated using Student's *t*-test. Pseudocolored images of Venus channel/CFP channel ratios of representative cells and a pseudocolor scale are shown. In the graph on the right, each plot indicates the Venus/CFP ratio of each cell. The horizontal lines in the center represent the mean values for each group.
doi:10.1371/journal.ppat.1002561.g002

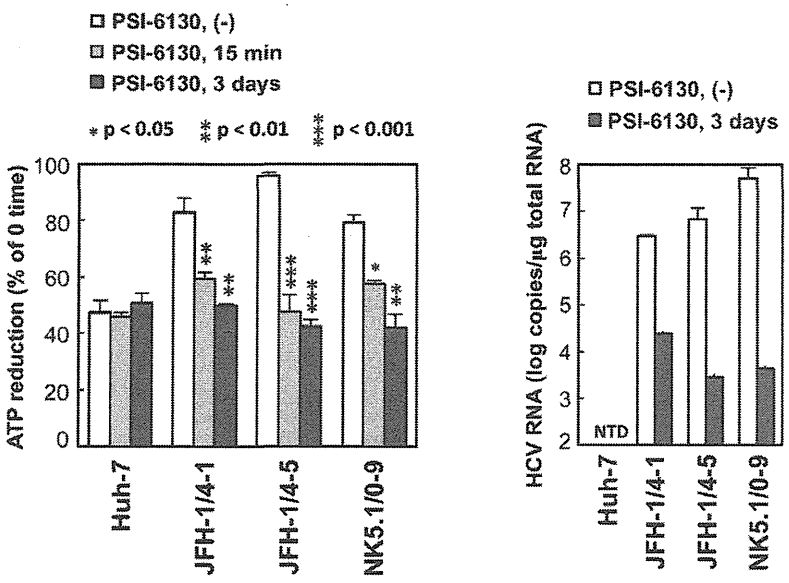

Figure 3. ATP consumption in cells replicating HCV RNA. (Left) The indicated cell lines were pretreated with 10 μM PSI-6130 for 3 days or were cultured in the absence of the drug, followed by trypsinization and permeabilization. ATP-containing reaction buffer plus 10 μM PSI-6130 was added to some of the non-pre-treated cells (PSI-6130, 15 min; light gray bars). ATP-containing PSI-6130-free reaction buffer was added to the rest of the non pre-treated cells (PSI-6130, (−); white bars) and to the pre-treated cells (PSI-6130, 3 days; dark gray bars). After 15 min incubation, ATP levels in cell lysates were measured using a luciferase-based assay. ATP reduction compared to ATP levels at the 0-time point was calculated. The mean values of three independent samples with SD are displayed. Statistical differences between cells treated with and without treatment with PSI-6130 were evaluated using Student's *t*-test. (Right) HCV RNA titers in cells corresponding to the left panel were determined using real-time quantitative RT-PCR. Data are presented as means and SD for three independent samples. NTD indicates not detected.
doi:10.1371/journal.ppat.1002561.g003

well as plasmids expressing NS5A-ATeam fusion proteins (NS5A-ATeam)(Figures 4A and 4C).

We first tested whether NS5A-ATeam fusion proteins can be used to monitor ATP levels over a range of concentrations in living cells. The Venus/CFP ratios in individual cells expressing NS5A fused either with AT1.03^{YEMK} (Kd = 1.2 mM at 37°C [2]) or with a relatively lower affinity version, AT1.03 (Kd = 3.3 mM at 37°C [2]) were measured. As shown in Figure 4B, differences in the Venus/CFP ratios of NS5A- AT1.03^{YEMK} and NS5A-AT1.03 were similar to those of AT1.03^{YEMK} and AT1.03, although average ratios were lower for NS5A- AT1.03^{YEMK} and NS5A-AT1.03 compared to AT1.03^{YEMK} and AT1.03. In the presence of 2DG and OliA, Venus/CFP ratios of NS5A-AT1.03^{YEMK} were markedly reduced to levels that were comparable to those of AT1.03^{RK}, an inactive mutant with R122K/R126K substitutions [2]. These results demonstrate that NS5A-ATeams can function as ATP indicators, although their dynamic ranges of Venus/CFP ratios are slightly smaller than those of the original, non-fused ATeams.

We next investigated whether the SGR-ATeam could initiate and sustain transient replication of HCV RNA in cells. A RNA polymerase I (Pol I)-derived plasmid, which carries SGR/luc-AT1.03 containing a luciferase reporter gene ([26]; Figure 4C), or its replication-defective mutant were transfected into Huh-7 cells and levels of viral replication were determined by measuring luciferase activity at various time intervals over a five day period (Figure 4D). Although replication of SGR/luc-AT1.03 was delayed compared with parental SGR/luc, the luciferase activity expressed from SGR/luc-AT1.03 rose to approximately a thousand-fold higher than that expressed from SGR/luc-GND-AT1.03 at five days post-transfection. It appears that SGR-AT1.03, which does not carry the luciferase gene, replicated more efficiently than SGR/luc-AT1.03, as determined by Western blotting of the HCV NS5B protein within cells four days post-transfection (Figure 4E). As indicated in Figure 4F, an abundant protein of the same size as that expected for the NS5A-ATeam fusion protein was observed in cells expressing either NS5A-AT1.03 or SGR-AT1.03, indicating that the NS5A-ATeam fusion protein is stable and is not cleaved during HCV replication. Thus, we concluded that the modified replicon constructs in which the ATeam is incorporated into the NS5A region are functional and remain capable of efficient transient replication of HCV RNA.

Visualization of ATP levels and distinctive features of ATP distribution in cells replicating ATeam-tagged SGR

This SGR-ATeam system that was established to analyze cellular ATP levels was used in living HCV RNA-replicating cells in which membrane-associated RCs are formed through the interaction of viral proteins, including NS5A, and cellular proteins. We compared the subcellular distribution of fluorescent signals expressed from NS5A-ATeams and SGR-ATeams using emission-scanning confocal fluorescence microscopy with a Zeiss META detector. NS5A-AT1.03 and NS5A-AT1.03^{YEMK} were diffusely distributed throughout the cytoplasm (Figure 5A; upper panels). Venus/CFP ratios of NS5A-ATeam constructs were almost constant throughout the cytoplasm (Figure 5A; lower). As expected, Venus/CFP ratios in cells expressing NS5A-AT1.03^{YEMK} were markedly higher than those of NS5A-AT1.03 (Figure 5A; lower). In contrast, cells replicating SGR-AT1.03 and SGR-AT1.03^{YEMK} showed foci of brightly fluorescent dot-like structures in the cytoplasm (Figure 5B; upper panels). Interestingly, some of these fluorescent foci had an apparently higher Venus/

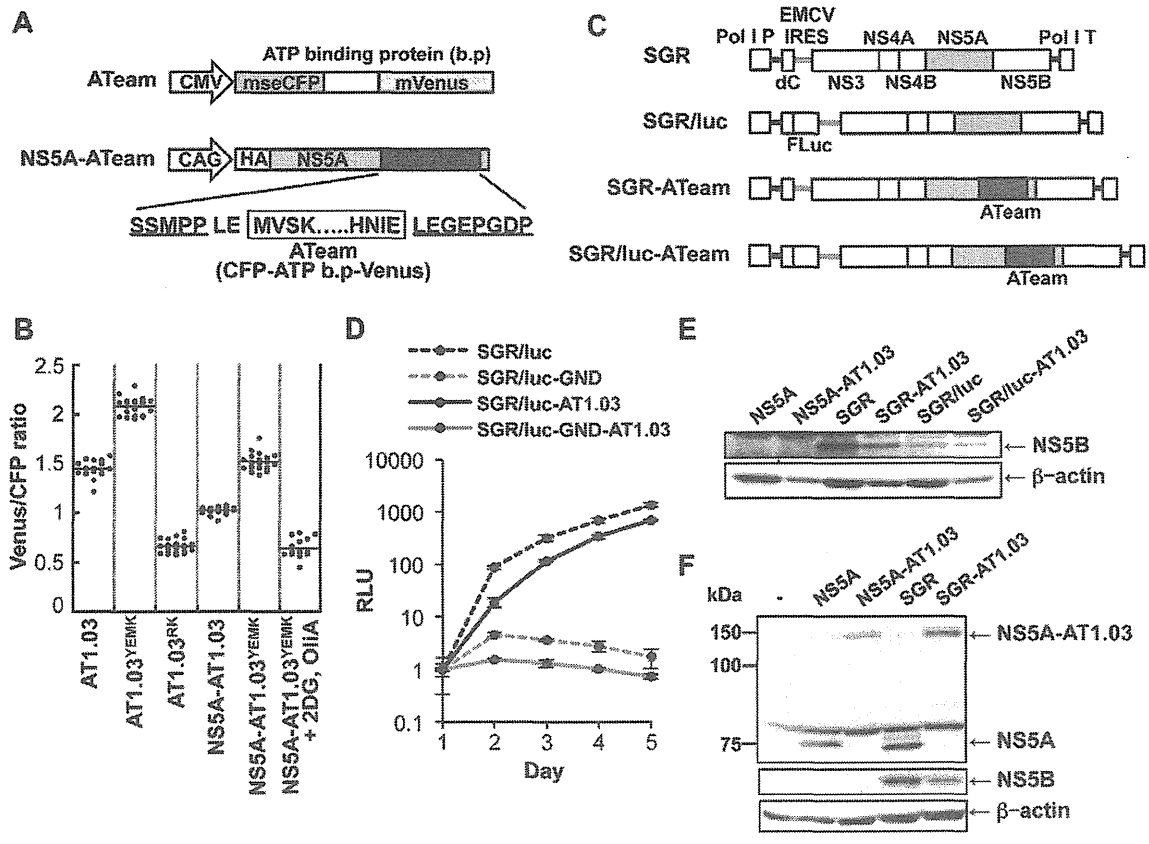

Figure 4. Development of NS5A-ATeam and SGR-ATeam to enable real-time monitoring of ATP. (A) Schematic representation of the ATeam and NS5A-ATeam used in this study. ATeam genes were inserted into the 3′ region of a HA-NS5A expression vector to generate NS5A-ATeam. The underlined sequences indicate NS5A residues. The insertion site was between residues 2394 and 2395, numbered according to the polyprotein of the HCV JFH-1 isolate. *CMV, Cytomegalovirus promoter; CAG, CAG promoter; ATP b.p, ATP binding protein. HA, HA tag.* (B) Huh-7 cells were transfected with ATeam and NS5A-ATeam constructs. Forty-eight hours post-transfection, the Venus/CFP ratios of each cell were calculated from fluorescent images acquired with a confocal microscope in the same way as described in the legends for Figure 2. Each plot shows the ratio of individual cells. Horizontal lines represent means. (C) Schematic representation of the SGR and SGR-ATeam plasmids used, with or without the firefly luciferase gene (Fluc). HCV polyproteins are indicated by the open boxes. ATeam genes were inserted into the same site in the NS5A C-terminal region. Bold lines indicate the HCV UTR. EMCV IRES is denoted by the gray bars. Pol I P, Pol I promotor; dC, 5′ region of Core gene; Pol I T, Pol I terminator. (D) Replication levels of SGR/luc-AT1.03 in transfected cells were determined by luciferase assay 1–5 days post-transfection. SGR/luc and SGR/luc-GND were used as positive and negative controls, respectively. Values given were normalized for transfection efficiency with luciferase activity determined 24 h post-transfection. All data are presented as means and SD for three independent samples. (E) Huh-7 cells were transfected with constructs encoding NS5A, NS5A-AT1.03, SGR, SGR-AT1.03, SGR/luc or SGR/luc-AT1.03, followed by immunoblotting with anti-NS5B or anti-beta-actin antibody. (F) Cells transfected with constructs encoding NS5A, NS5A-AT1.03, SGR or SGR-AT1.03 were analyzed by immunoblotting with anti-NS5A, anti-NS5B or anti-beta-actin antibodies.
doi:10.1371/journal.ppat.1002561.g004

CFP ratio than the surrounding cytoplasmic region (Figure 5B; middle and lower panels). Although the number of high Venus/CFP ratios was not consistent between the cells, this phenotype was observed in most of the cells that were replicating SGR-AT1.03 (Figure S3). Such high focal Venus/CFP ratios were not detected in cells replicating SGR-AT1.03^{RK} or in SGR-AT1.03^{YEMK} -replicating cells treated with 2DG and OliA. Thus, foci with a high Venus/CFP ratio apparently represent the presence of high ATP levels at distinct sites in cells replicating HCV RNA. In addition, when a replication-defective polyprotein that extended from NS3 through to the NS5B protein, including NS5A-AT1.03, was expressed, no high Venus/CFP ratio was seen in the cells in spite of the fact that NS5A-AT1.03 was detected in dot-like structures throughout the cytoplasm (Figure S4). These results strongly suggest that the high Venus/CFP ratios observed using the SGR-ATeam system are associated with the replication of HCV RNA.

To investigate whether the high Venus/CFP ratios of the dot-like structures detected in cells replicating SGR-ATeam are located at the HCV RC, FRET images of SGR-AT1.03-replicating cells were analyzed, followed immunofluorescence analysis of cells fixed and stained with either anti-NS5A or anti-NS3 antibodies (Figure 5C). Confocal fluorescence microscopy at high magnification demonstrated that the high Venus/CFP ratios that were identified in foci of various sizes were co-localized with NS5A and NS3 that were possibly membrane-bound within the cytoplasm of the viral replicating cells. Some of the NS3- or NS5A-labeled proteins that were identified by immunofluorescence were not associated with high Venus/CFP ratios. These results are consistent with previous reports, which demonstrated that only

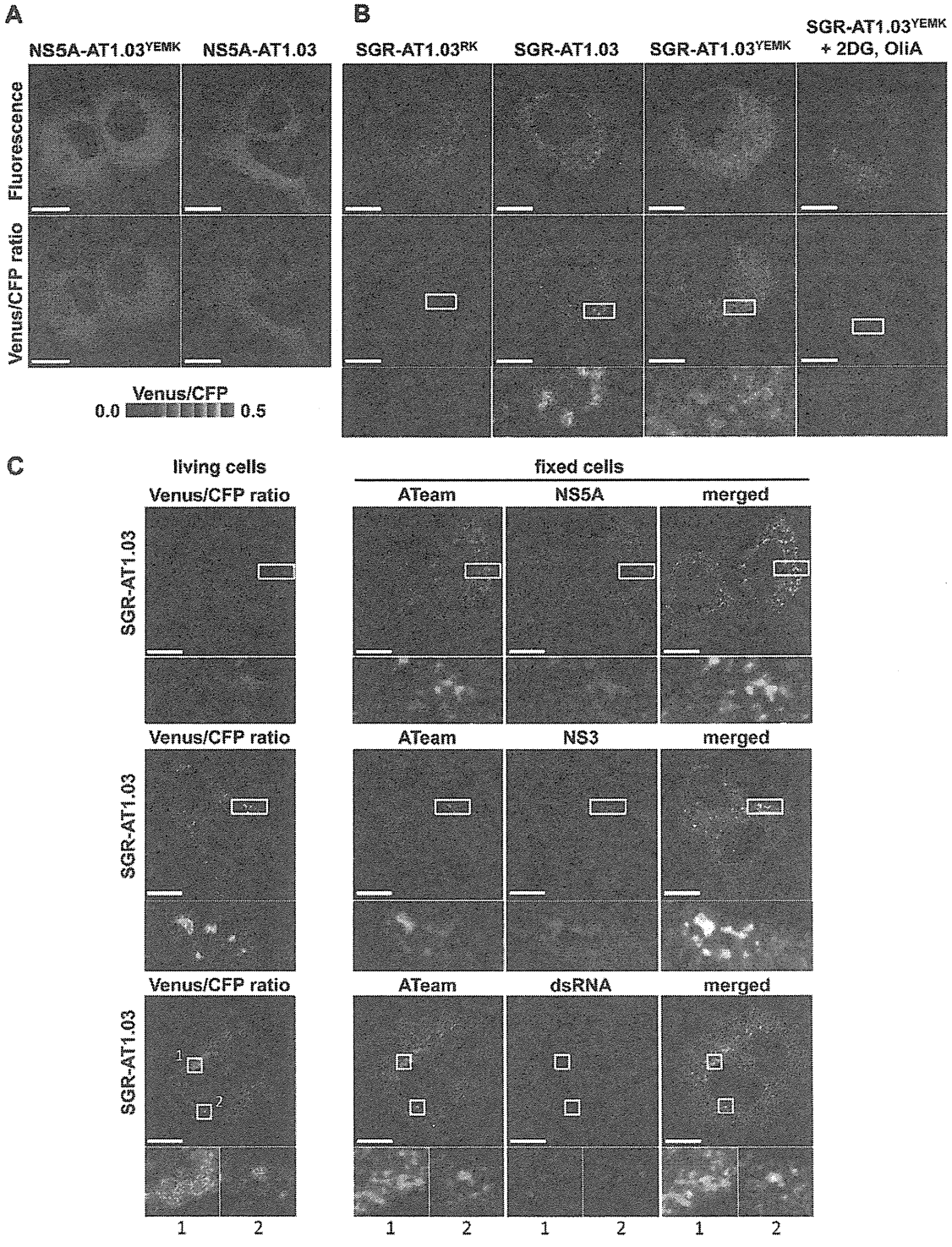

Figure 5. Visualization of sites of focal accumulation of ATP in cells expressing NS5A-ATeam or SGR-ATeam. (A) Huh-7 cells were transfected with NS5A-AT1.03 or NS5A-AT1.03^{YEMK}. Four days after transfection, the cells were analyzed using spectral imaging (405-nm excitation) of LSM510-META (Carl Zeiss). Images were processed to the CFP channel (F_{CFP}) and the Venus channel (F_{Venus}) using a linear unmixing algorithm using a reference for each spectrum. The upper panels demonstrate the signal intensity from a spectral channel with maximum intensity and represent the expression pattern of NS5A-ATeam. The lower panels are constructed from FRET ratio images (F_{CFP}/F_{Venus}) with pseudocolors. The pseudocolor scale is shown below. Scale bars, 20 μm. (B) Huh-7 cells were transfected with SGR-AT1.03^{RK}, SGR-AT1.03 or SGR-AT1.03^{YEMK}, and were analyzed in the same

way as described in (A). SGR-AT1.03^{YEMK} -transfected cells were treated with 10 mM 2DG and 10 μg/ml OliA just before imaging and were used as a negative control. The upper panels demonstrate the intensity from a spectral channel with maximum intensity and represent the expression pattern of NS5A-ATeam processed from SGR-ATeam. The lower panels indicate square areas within FRET ratio panels magnified five-fold. Scale bars, 20 μm. (C) Cells were fixed after live-cell FRET imaging, and the same cell was analyzed by indirect immunofluorescence staining. Viral proteins were labeled with antibodies against NS5A (upper panels), NS3 (middle panels) and dsRNA (lower panels), which were detected with an Alexa Fluor 555-labeled anti-rabbit or anti-mouse antibody. ATeam panels (green) represent the expression of NS5A-ATeam processed from SGR-ATeam, and NS5A, NS3 or dsRNA panels (red) represent the immunostained signals. Enlarged views of the areas outlined by squares at a five-fold magnification are also shown. Scale bars, 20 μm.
doi:10.1371/journal.ppat.1002561.g005

some of the expressed HCV NS proteins contribute to viral RNA synthesis [27]. To further investigate the relationship between the cellular sites at which there was a high Venus/CFP ratio and HCV RNA replication, double-stranded RNA (dsRNA) was visualized by staining with a specific anti-dsRNA antibody after FRET imaging (Figure 5C). This staining indicated that dsRNA-containing dot-like structures co-localized with structures that displayed high Venus/CFP ratios. Therefore, it is most likely that the dot-like structures with high Venus/CFP ratios that were detected using the SGR-ATeam system reflect the sites of HCV RNA replication or HCV RCs.

Several studies have shown that mitochondria, which play a central role in ATP metabolism, localize to areas near the membranous web, the likely site of HCV RNA replication [28]. We thus compared the subcellular localization of the fluorescence signals detected in cells expressing SGR-ATeam with that of mitochondria that were visualized by staining with Mitotracker. Foci with high Venus/CFP ratios did not colocalize with, but were localized adjacent to mitochondria in cells that were replicating SGR-AT1.03 (Figure S5). This finding might reflect the fact that ATP can be directly supplied from mitochondria to the sites of viral RNA replication in cells.

Quantification of ATP at putative cytoplasmic sites of HCV RNA replication within cells

Based on the above observations, FRET signals detected within cells expressing SGR-ATeam or NS5A-ATeam can be classified as either signals from distinct dot-like structures, which represent putative subcellular sites of HCV RNA replication, or as signals that are diffuse throughout the cytoplasm. The Venus/CFP emission ratio in individual cells into which NS5A-AT1.03, NS5A-AT1.03^{YEMK}, SGR-AT1.03, SGR-AT1.03^{YEMK} or SGR-AT1.03^{RK} was introduced was determined (Figure 6A). Fluorescent signals corresponding to cytoplasmic ATP were identified by subtracting signals at putative sites of viral RNA replication from signals from the cytoplasmic area as a whole. Cytoplasmic Venus/CFP ratios within cells replicating SGR-AT1.03 and SGR-AT1.03^{YEMK} were lower than those in cells expressing NS5A-AT1.03 and NS5A-AT1.03^{YEMK}, respectively. Therefore, cytoplasmic ATP levels within HCV RNA-replicating cells were lower than in non-replicating cells. This result is consistent with the findings shown in Figure 1A. The average Venus/CFP ratios at potential sites of viral RNA replication were greater than the corresponding cytoplasmic levels in cells replicating SGR-AT1.03 or SGR-AT1.03^{YEMK}. As expected, a significant decrease in Venus/CFP ratios was observed in cells treated with 2DG and OliA.

We next quantified ATP levels within individual cells replicating HCV RNA based on the Venus/CFP ratios obtained. To generate standard curves for this calculation, permeabilized cells expressing NS5A-AT1.03 or NS5A-AT1.03^{YEMK} were prepared by digitonin treatment, followed by the addition of defined concentrations of ATP and subsequent FRET analysis [29,30]. As shown in Figure 6B, under these experimental conditions, baseline Venus/CFP ratios of approximately 0.1 were detected in the absence of exogenous ATP, and Venus/CFP ratios were observed to increase linearly with increasing ATP concentration. The standard curves thus obtained can be used to estimate the ATP concentrations of unknown samples in which a particular ATeam containing an ATP probe at the C terminus of HCV NS5A, such as NS5A-ATeam or SGR-ATeam, have been introduced. Based on the fluorescent signal obtained in cells replicating SGR-ATeam, as well as in cells expressing NS5A-ATeam, the ATP concentration at putative sites of HCV RNA replication was estimated to be ~5 mM in the experiments shown in Figures 5A and 5B (average value of putative replication sites; 4.8 mM). After subtraction of the ATP that was localized at the HCV replication sites, the ATP concentration of HCV-replicating SGR cells (~1 mM) was found to be approximately half that observed in parental non-replicating cells (~2 mM)(average values in SGR and parental cells; 0.8 mM and 2.2 mM, respectively). To our knowledge, this is the first experiment in which ATP levels were estimated inside living cells during viral genome replication.

Figures 5 and 6A demonstrate changes in ATP concentrations at distinct sites in cells undergoing HCV RNA replication. Finally, we determined the effect of the PSI-6130 inhibitor of HCV replication on the change in subcellular ATP concentration in cells following introduction of SGR-AT1.03, SGR-AT1.03^{RK} or NS5A-AT1.03 (Figure 6C). In general, nucleoside analogue inhibitors of viral replication prevent RNA/DNA synthesis by chain termination immediately after addition to infected cells [23]. Indeed, as shown in Figure 3, a decrease in ATP consumption was detected even following a PSI-6130 treatment period as short as 15 min of permeabilized HCV replicon cells. We therefore analyzed and estimated ATP levels in cells in the presence of PSI-6130 for 10 min and 2 h. ATP concentrations at putative sites of viral RNA replication, as well as cytoplasmic ATP levels, were higher in SGR-AT1.03-replicating cells in the presence of 0.1–5 μM PSI-6130 for 10 min compared to the same cells without inhibitor treatment or to NS5A-AT1.03-expressing cells. A dose-dependent PSI-6130-induced increase in ATP levels at the putative replication sites was observed under the condition used. By treatment with PSI-6130 for 2 h, the ATP levels at putative replication sites were significantly lower than those without inhibitor treatment in SGR-AT1.03-replicating cells. The cytoplasmic ATP levels were similar with or without 2-h treatment (Figure 6C). In HCV SGR-ATeam cells treated with PSI-6130 for 3 days, HCV RNA replication was dramatically inhibited by greater than 90% with no observed cytotoxicity (Figure S6) and, as expected, little or no high Venus/CFP signal was detected anywhere in the cells (data not shown). We adapted the ATeam system to monitor ATP in HCV RNA replicating cells and found increased ATP levels at the putative subcellular sites of the viral replication. Findings obtained from experiments using the viral polymerase inhibitor strongly suggest that changes in ATP concentrations at the distinct sites observed depend on the viral RNA replication.

Discussion

This paper is the first to demonstrate changes in ATP within cells during viral genome replication. ATP requirements during

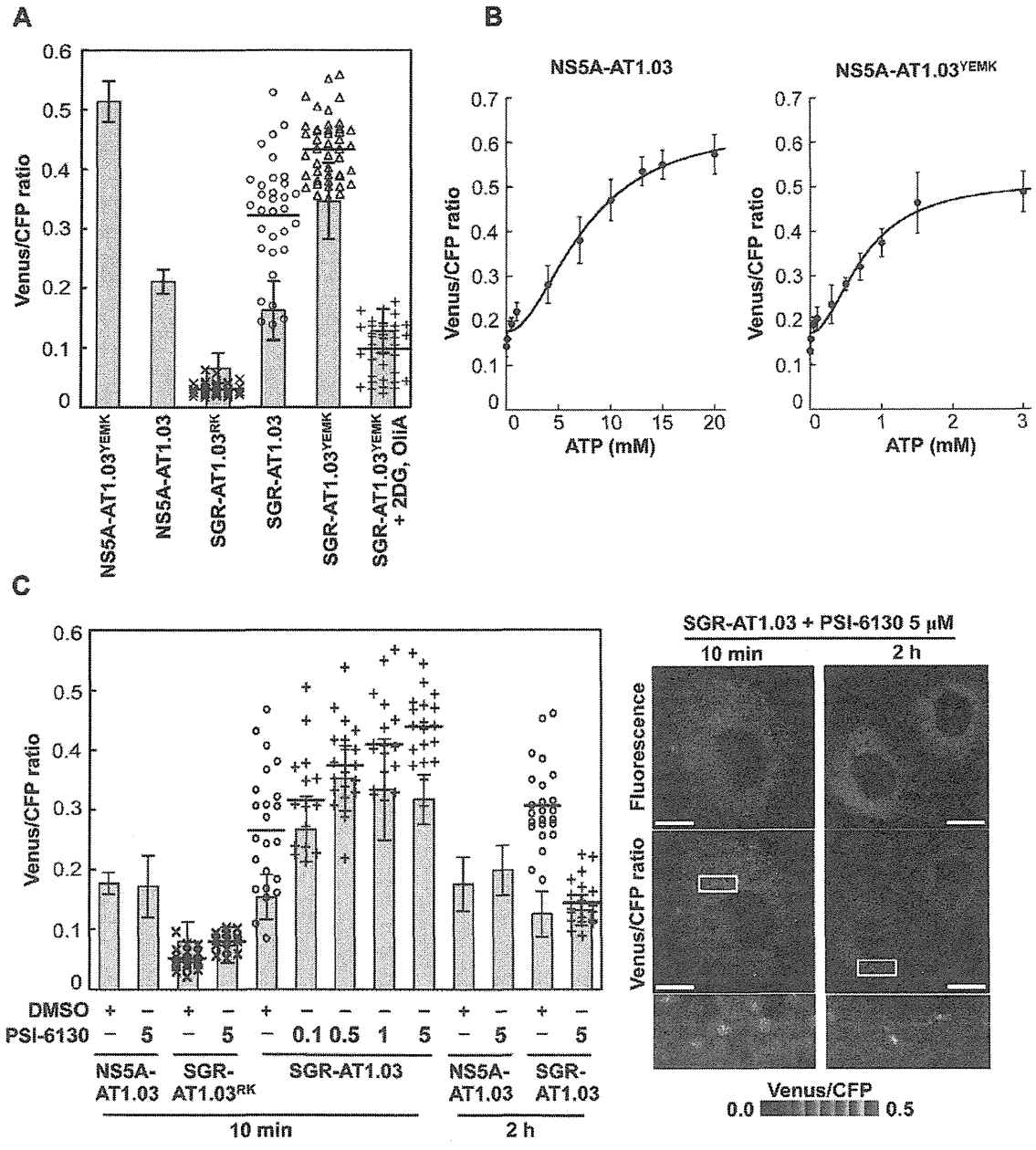

Figure 6. Estimation of ATP levels at possible sites of HCV RNA replication in living cells. (A) Venus/CFP emission ratios were calculated from images of CFP and Venus channels in individual cells for each group. Bar- and dotted graphs indicate ratios within the cytoplasm and ratios for dot-like structures, respectively, in the same cells, as shown in Figures 5A and 5B. Data in bar graphs are indicated as means and SD. Horizontal lines in the dot graphs denote means from at least three independent cells. Values in the cytoplasm of cells transfected with NS5A-AT1.03^{YEMK} and SGR-AT1.03^{YEMK} were statistically significant ($p<0.05$) as evaluated using the Student's *t*-test. (B) Calibration of NS5A-ATeam in cells under semi-intact conditions. Cells were transfected with NS5A-AT1.03 and NS5A-AT1.03^{YEMK}, respectively. Forty-eight hours later, the cells were permeabilized, followed by addition of known concentrations of ATP. FRET analyses were performed as described in Figure 5A. Each trace represents mean with SD of at least six independent cells. Plots were fitted with Hill equations with a fixed Hill coefficient of 2; $R=(R_{max}-R_{min})\times[ATP]^2/([ATP]^2+Kd^2)+R_{min}$, where R_{max} and R_{min} are the maximum and minimum fluorescence ratios, respectively. *Kd* is the apparent dissociation constant. R values were 0.994 and 0.986 for NS5A-AT1.03 and NS5A-AT1.03^{YEMK}, respectively. (C) Cells were transfected with NS5A-AT1.03, SGR-AT1.03^{RK} or SGR-AT1.03. The cells were then treated with PSI-6130 at indicated concentrations (μM) for 10 min or 2 h, and were analyzed as described in (A). Values in the cytoplasm of cells transfected with SGR-AT1.03 with and without PSI-6130 treatment were statistically significant ($p<0.05$ for control versus 0.1 or 1 μM PSI-6130, $p<0.01$ for control versus 0.5 or 5 μM PSI-6130) as evaluated using the Student's *t*-test. Representative cells treated with 5 μM PSI-6130 are shown in the right panel. The lower panel is a five-fold magnification of the boxed area. Scale bars, 20 μm.
doi:10.1371/journal.ppat.1002561.g006

the virus lifecycle have been studied for years. Several key steps during the viral life cycle, such as genome synthesis, require high-energy phosphoryl groups. For instance, it has been shown that ATP is required for the formation of a preinitiation complex for de novo RNA synthesis by RdRp of flaviviruses [31]. Transcriptional initiation and RNA replication by influenza virus RdRp are functional in an ATP-dependent fashion [32,33]. An ATP requirement of viral helicase activities has also been reported [34]. Furthermore, it has been demonstrated that ATP is involved in the assembly and/or release of viral structural proteins possibly via interaction with ATP-dependent chaperones [35,36]. However, it has been controversial as to whether ATP can be concentrated in particular subcellular compartment(s) in infected cells during viral replication. One of the underlying reasons for this controversy may be that a method by which cellular ATP levels can be determined, apart from examination of ATP levels in cellular extracts in the steady-state, has been lacking [37]. Recently Imamura et al. established FRET-based indicators, known as ATeams, for ATP quantification, and have shown that the use of ATeams enables the monitoring of ATP levels in real-time in different cellular compartments within individual cells [2].

In this study, in order to visualize and monitor ATP levels in living cells during replication of the viral genome, we first introduced the original ATeam-expressing plasmids into cells and found that cytoplasmic ATP levels in cells undergoing HCV genotype 1b and 2a RNA replication were lower than those in cured or parental cell lines (Figures 2 and S2). These results agree with the results of CE-TOF MS analysis (Figure 1) and the ATP consumption assay (Figure 3). It is therefore likely that ATP is actively consumed in cells during viral RNA replication, resulting in reduced levels of ATP in the cytoplasm. Furthermore, NS5A-ATeam fusion constructs, in which the ATeam gene was introduced into the C-terminal end of the NS5A coding region, and SGR-ATeam constructs containing a HCV JFH-1-derived subgenomic replicon within the NS5A-ATeam fused sequence as described above, were engineered (Figure 4). The results obtained using several ATeam fusion constructs with different affinities for ATP indicated that NS5A-ATeam fusion constructs can be used as FRET-based ATP indicators, and that the ATeam-tagged HCV replicons are capable of transient replication of viral RNA (Figure 4). It is interesting that our experiment using a SGR-ATeam construct provides evidence for the formation of ATP-enriched foci within cells that support HCV RNA replication (Figures 5 and 6). FRET-signal detection followed by indirect immunofluorescence allowed us to visualize co-localization of viral proteins as well as dsRNA at sites of ATP accumulation in cells (Figure 5), suggesting that these membrane-associated ATP-enriched foci likely represent sites of HCV RNA replication in transient replication assays.

Attempting to precisely quantify ATP within individual cells or particular intracellular compartments is a very challenging process. The luciferin-luciferase reaction has been utilized to monitor cellular ATP levels by measuring the released photon count during catalysis of bioluminescent oxidation by firefly luciferase. A previous study based on the luciferin-luciferase assay estimated basal cytoplasmic ATP levels at ~1.3 mM, which increased to ~5 mM during apoptotic cell death [38]. However, the results obtained were likely influenced by cellular levels of luciferase and other assay components, as well as by the pH of the cells. In this study, we describe quantification of ATP in human hepatoma Huh-7 cells undergoing HCV RNA replication using SGR-ATeam technology. Although ATP requirements during the lifecycles of various viruses have been studied for years, the use of ATeam technology enabled us, for the first time, to evaluate ATP concentrations at sites of viral replication within living cells. We here demonstrate that ATP concentrations at these putative subcellular sites of HCV RNA replication approach ~5 mM (Figure 6). This ATP level is as high as that observed during apoptotic processes such as caspase activation and DNA fragmentation, even though the latter ATP level was determined using a different assay system [38]. Considering that these apoptotic events were not observed at basal ATP levels [38], replication of the viral genome likely also requires high concentrations of cellular ATP. It should be noted that, in contrast to the fluorescent reporter system traditionally used to calculate the ATP/ADP ratio [39], the bacterial epsilon subunit used in ATeam is highly specific for ATP, but not for other nucleotides such as ADP, CTP, GTP or UTP [2,3]. In evaluating the effect of the HCV polymerase inhibitor on changes in the subcellular ATP concentration in cells replicating SGR-ATeam, an increase in ATP concentration was observed both at putative replication sites and in the cytoplasm of SGR-AT1.03-replicating cells in the presence of PSI-6130 for 10 min (Figure 6C). By contrast, 2-h treatment with the inhibitor resulted in reduction of ATP levels at putative replication sites in the replicon cells. Although the result of the experiment with 10-min treatment may be somewhat unexpected, it might possibly be explained by the following hypothesis. PSI-6130 began to inhibit viral RNA synthesis, leading to a decrease in ATP consumption. Since a mechanism for ATP transport mediated by host cell and/or viral factor(s) is still active during this time period, the ATP level at the replication sites should be increased compared to that during active replication. Higher levels of metabolic intermediates for glyconeogenesis as well as for glycolysis in HCV-infected cells compared to non-infected cells as determined via metabolome analysis (data not shown) may also be implicated in the increased ATP levels at the initial stage of inhibition of HCV replication. It is likely that active consumption of ATP caused by HCV replication and ATP transportation into the replication sites would lead to reduction of cytoplasmic ATP level. Such a change in ATP balance may result in induction of ATP generation and increase in certain metabolic intermediates related to glucose metabolism. These metabolome responses are supposed to maintain in short-term (10 min) treatment with PSI-6130. Thus, inhibition of HCV RNA replication by PSI-6130 under the conditions used may lead to increase in the cytoplasmic ATP level. It is likely that these metabolome responses were not observed after the longer-term (2 h) treatment presumably because the viral replication was inhibited by the inhibitor for a sufficient period of time. Further study is required to address the molecular mechanism underlying change in ATP balance caused by HCV replication and the viral inhibitors.

The mechanism by which ATP accumulates at potential sites of HCV RNA replication remains unclear. We have previously demonstrated that creatine kinase B (CKB), which is an ATP-generating enzyme and maintains cellular energy stores, accumulates in the HCV RC-rich fraction of viral replicating cells [22]. Our earlier results suggest that CKB can be directed to the HCV RC via its interaction with the HCV NS4A protein and thereby functions as a positive regulator for the viral replicase by providing ATP [22]. One may hypothesize that recruitment of the ATP generating machinery into the membrane-associated site, through its interaction with viral proteins comprising the RC, is at least in part linked with elevated concentrations of ATP at a particular site. Through our preliminary study, however, subcellular ATP distribution was not changed significantly in replicon cells where HCV RNA replication was reduced ~50% by siRNA-mediated knockdown of the CKB gene (data not shown). Another possibility

may be implication of communication between mitochondria and membrane-enclosed structures of HCV RC in ATP transport through membrane-to-membrane contact. As indicated in Figure S5, putative sites of the viral RNA replication with high Venus/CFP ratios were mainly localized proximal to mitochondria. Studies are ongoing to understand the mechanism(s) underlying this phenomenon, as well as to determine if changes in ATP levels at intracellular sites supporting replication might also be observed for other RNA or DNA viruses.

In summary, we have used a FRET-based ATP indicator called ATeam to monitor ATP levels in living cells where viral RNA replicates by designing HCV replicons harboring wild-type or mutated ATeam probes inserted into the C-terminal domain of NS5A. We evaluated changes in ATP levels during HCV RNA replication and demonstrated elevated ATP levels at putative sites of replication following detection of FRET signals, which appeared as dot-like foci within the cytoplasm. The ATeam system may become a powerful tool in microbiology research by enabling determination of subcellular ATP localization in living cells infected or associated with microbes, as well as investigation of the regulation of ATP-dependent processes during the lifecycle of various pathogens.

Materials and Methods

Chemicals

PSI-6130 (β-D-2′-Deoxy-2′-fluoro-2′-*C*-methylcytidine) and recombinant human IFN-alpha2b were obtained from Pharmasset Inc. (Princeton, NJ) [23,24] and Schering-Plough (Kenilworth, NJ), respectively. OliA and 2DG were purchased from Sigma-Aldrich (St. Louis, MO). ATP used in this study was complexed with equimolar concentrations of magnesium chloride before use in the experiments.

Plasmids

The construction of the ATeam plasmids pRSET-AT1.03, pRSET-AT1.03^{YEMK} and pRSET-AT1.03$^{R122K/R126K}$, which express wild-type ATeam (AT1.03), as well as a high-affinity mutant (AT1.03^{YEMK}) and a non-binding mutant (AT1.03^{RK}), has been previously described [2]. pHH/SGR-Luc (also termed SGR/luc) contains cDNA of a subgenomic replicon of HCV JFH-1 isolate (genotype 2a; [14]) with firefly luciferase flanked by the Pol I promoter and the Pol I terminator, yielding efficient RNA replication upon DNA transfection [26]. pHH/SGR-Luc/GND (also termed SGR/luc-GND), in which a point mutation of the GDD motif of the NS5B was introduced in order to abolish RNA-dependent RNA polymerase activity, was used as a negative control. pHH/SGR (also termed SGR) was created by deleting the luciferase gene in pHH/SGR-Luc. To generate a series of SGR-ATeam plasmids, wild-type or mutant ATeam genes were inserted into pHH/SGR-Luc or pHH/SGR at the Xho I site of NS5A (between amino acids 418 and 419) [25]. The ATeam genes were also inserted into the same site of pCAGNS5A, which contains the NS5A gene of JFH-1 downstream of the CAG promoter and hemagglutinin (HA) tag [26], yielding NS5A-ATeam plasmids. To generate a plasmid expressing NS3-NS5B-AT1.03 under the control of the CAG promoter, a DNA fragment containing the coding region of NS3/NS4A/NS4B/NS5A-AT1.03/NS5B of SGR/luc-ATeam was inserted into the pCAGGS vector [40]. Exact cloning strategies are available upon request.

Cell culture and plasmid transfection

Human hepatoma Huh-7 cells were propagated in Dulbecco's modified Eagle's medium (DMEM) supplemented with 10% fetal calf serum (FCS) as well as minimal essential medium non-essential amino acid (MEM NEAA)(Invitrogen, Carlsbad, CA) in the presence of 100 units/ml of penicillin and 100 μg/ml of streptomycin. The Huh-7-derived cell lines JFH-1/4-1 and JFH-1/4-5, which support replication of SGR RNA of HCV JFH-1 (genotype 2a) and NK5.1/0-9, which carries the SGR RNA of Con1 NK5.1 (genotype 1b), were cultured and maintained under previously described conditions [15]. DNA transfection was performed using a TransIT-LT1 transfection reagent (Takara, Shiga, Japan) in accordance with the manufacturer's instructions.

CE-TOF MS analysis

Huh-7 cells were mock-infected or infected with HCVcc derived from a wild-type JFH-1 isolate at a multiplicity of infection of 1. When most cells had become virus positive, as confirmed by immunofluorescence, with no observable cell damage at 9 days post-infection, equal amounts of cells with and without HCV infection were scraped with MeOH including 10 μM of an internal standard after washing twice with 5% mannitol solution. Replicon cells (JFH-1/4-5) that were cultured in the absence of G418 for 2 days were harvested and prepared as above. The extracts were mixed with chloroform and water, followed by centrifugation at 2,300× *g* for 5 min at 4°C, The upper aqueous layer was centrifugally filtered through a 5-kDa cutoff filter to remove proteins. The filtrate was lyophilized and dissolved in water, then subjected to CE-TOF MS analysis. CE-TOF MS experiments were performed using an Agilent CE-TOF MS system (Agilent Technologies, Waldbronn, Germany) as described previously [41].

ATP consumption assay

The ATP consumption assay using permeabilized replicon cells was carried out as previously described [13,22] with slight modifications, so that it was unnecessary to add either exogenous phosphocreatine or creatine phosphokinase to minimize ATP reproduction in cells. Cells (2×10^6) cultured in the presence or absence of PSI-6130 for 72 h were treated with 5 μg Actinomycin D/ml, followed by trypsinization and 3 washes with cold buffer B (20 mM HEPES-KOH [pH 7.7], 110 mM potassium acetate, 2 mM magnesium acetate, 1 mM EGTA, and 2 mM dithiothreitol). The cells were permeabilized by incubation with buffer B containing 50 μg/ml digitonin for 5 min on ice and the reaction was stopped by washing 3 times with cold buffer B. The permeabilized cells (1×10^5) were resuspended with 100 μl buffer B containing 5 μM ATP, GTP, CTP, and UTP, 20 μM $MgCl_2$, and 5 μg/ml Actinomycin D. After incubation at 27°C for 15 min, samples were centrifuged, and 20 μl of the supernatant was then mixed with 5 μl of 5× passive lysis buffer (Promega, Madison, WI). The ATP level was determined using a CellTiter-Glo Luminescent cell viability assay system (Promega). All assays were performed at least in triplicate.

Live cell microscopy

Plasmids carrying the ATP indicators were transfected at 48 h (ATeam and NS5A-ATeam) or 4 days (SGR-ATeam) before imaging of the cells. One day before imaging, the cells were seeded onto 30-mm glass-bottomed dishes (AGC Techno Glass, Chiba, Japan) at about 60% confluency. For imaging, the cells were maintained in phenol red-free DMEM containing 20 mM HEPES-KOH [pH 7.7], 10% FCS and MEM NEAA.

Two kinds of confocal microscopies were used to perform the FRET analysis in this study as follows. Since the ways of acquisition of each spectrum were quite different between the two microscopies, differences in the values of the Venus/CFP ratios in different

experiments were observed. In Figures 2, 4B and S2, cells were imaged using a confocal inverted microscope FV1000 (Olympus, Tokyo, Japan) equipped with an oil-immersion 60× Olympus UPlanSApo objective (NA = 1.35). Cells were maintained on the microscope at 37°C with a stage-top incubation system (Tokai Hit, Shizuoka, Japan). Cells were excited by a 405-nm laser diode, and CFP and Venus were detected at 480–500 nm and 515–615 nm wavelength ranges, respectively. In the analysis shown in Figures 5, 6, S3, S4 and S5, FRET images were obtained using a Zeiss LSM510 Meta confocal microscope with an oil-immersion 63× Zeiss Plan-APOCHROMAT objective (NA = 1.4)(Carl Zeiss, Jena, Germany). Cells were maintained on the microscope at 37°C with a continuous supply of a 95% air and 5% CO_2 mixture using a XL-3 incubator (Carl Zeiss). Cells were excited by a 405-nm blue diode laser, and emission spectra of 433–604 nm wavelength range were obtained using an equipped scanning module (META detector) [42,43]. Images were computationally processed by a linear unmixing algorithm using the reference spectrum of CFP and Venus, which were obtained from individual fluorescence-expressing cells. All image analyses were performed using MetaMorph (Molecular Devices, Sunnyvale, CA). Fluorescence intensities of cytoplasmic areas in NS5A-ATeam transfected cells were calculated by subtraction of the signal intensities of the nucleus from the signal intensities of the whole cell, which was standardized by the area of the corresponding cytoplasmic region. Fluorescence intensities of cytoplasmic areas and at dot-like structures corresponding to the putative viral replicating sites in SGR-ATeam-transfected cells were measured and calculated as follows. All pixels above CFP intensity levels of 100–200 were selected. The positions of dot-like structures were then determined by examining areas greater than 0.5×10^{-12} square meters and the intensity of each dot was measured. The fluorescence intensity of the cytoplasmic area, excluding that of the putative viral replicating sites in each cell, was calculated by subtraction of the signal intensities of the nucleus and the dot-like structures, as determined above, from the signal intensity of the whole cell, which was standardized by the area of the corresponding cytoplasmic region. Each Venus/CFP emission ratio was calculated by dividing pixel-by-pixel a Venus image with a CFP image.

To investigate the relationship between Venus/CFP ratios and ATP concentrations in cells, calibration procedures were performed according to previous reports [29,30]. Huh-7 cells were transfected with NS5A-AT1.03 or NS5A-AT1.03^{YEMK}. Forty-eight hours later, the cells were permeabilized by incubation with buffer B containing 50 μg/ml digitonin for 5 min at room temperature. The reaction was stopped by washing 3 times with buffer B, followed by the addition of known concentrations of ATP in warmed medium for imaging. FRET analysis, with calibration of the signal intensity in the cytoplasm of each cell, was performed as described above. Plots were fitted with Hill equations with a fixed Hill coefficient of 2; $R = (R_{max}-R_{min})\times[ATP]^2/([ATP]^2+Kd^2)+R_{min}$, where R_{max} and R_{min} are the maximum and minimum fluorescence ratios, respectively and Kd is the apparent dissociation constant.

To analyze the effect of an inhibitor against HCV NS5B polymerase, the medium for the cells replicating SGR-ATeam was changed to medium containing various concentrations of PSI-6130. After 10-min incubation at 37°C under a continuous supply of 95% air and 5% CO_2, fluorescence intensities of cytoplasmic areas and at dot-like structures were determined as described above. Medium containing 0.01% DMSO was used as a negative control.

To visualize mitochondria, MitoTracker Red CMXRos (Molecular Probes, Eugene, OR) was added to the culture medium to a final concentration of 100 nM, incubated for 15 min at 37°C and the cells were then washed twice with phosphate buffered saline (PBS) before FRET analysis of living cells. Images were computationally processed as described above. The reference spectrum of MitoTracker Red CMXRos was obtained from stained parental, non-transfected, Huh-7 cells.

Indirect immunofluorescence

Cells expressing SGR-ATeam were cultured in 30-mm glass-bottomed dishes with an address grid on the coverslip (AGC Techno Glass). After FRET analysis of living cells as described above, the cells were fixed with 4% paraformaldehyde at room temperature for 30 min. After washing with PBS, the cells were permeabilized with PBS containing 0.3% Triton X-100 and individually stained with a rabbit polyclonal antibody against NS3 [44], an anti-NS5A antibody [45], or a mouse monoclonal antibody against dsRNA antibody (Biocenter Ltd., Szirak, Hungary) [46]. The fluorescent secondary antibody used was Alexa Fluor 555-conjugated anti-rabbit- or anti-mouse IgG (Invitrogen). The cells were imaged using a Zeiss LSM510 Meta confocal microscope with an oil-immersion 63× Zeiss Plan-APOCHROMAT objective (NA = 1.4). For dual-color imaging, the ATeam signal was excited with the 488-nm laser line of an argon laser and Alexa Fluor 555 was excited with a 543-nm HeNe laser under MultiTrack mode. Emission filters with a 505- to 530-nm band-pass and 560-nm-long pass filter were used.

Luciferase assay

Huh-7 cells transfected with SGR/luc or SGR/luc-ATeam were harvested at different time points after transfection (Figure 4D) or at 3 days after treatment with PSI-6130 (Figure S6) and lysed in passive lysis buffer (Promega). To monitor HCV RNA replication, the luciferase activity in cells was determined using a Luciferase Assay system (Promega). All assays were performed at least in triplicate.

MTT assay

Cell viability was assessed using the Cell Proliferation Kit II (Roche, Indianapolis, IN) according to the manufacturer's instructions. The kit measures mitochondrial dehydrogenase activity, which is used as a marker of viable cells, using a colorimetric sodium3′-[1(-phenylaminocarbonyl)-3,4-tetrazolium]-bis(4-methoxy-6-nitro)benzene sulfonic acid hydrate (MTT) assay.

Quantification of HCV RNA

HCV RNA copies in the replicon cells with or without PSI-6130 treatment were determined using the real-time detection reverse transcription polymerase chain reaction (RTD-PCR) described previously [47] with the ABI Prisom 7700 sequence detector system (Applied Biosystems Japan, Tokyo, Japan).

Western blotting

The proteins were transferred onto a polyvinylidene difluoride membrane (Immobilon; Millipore, Bedford, MA) after separation by SDS-PAGE. After blocking, the membranes were probed with a rabbit polyclonal anti-NS5A antibody [44], a rabbit polyclonal anti-NS5B antibody (Chemicon, Temecula, CA), or a mouse polyclonal anti-beta-actin antibody (Sigma-Aldrich), followed by incubation with a peroxidase-conjugated secondary antibody and visualization with an ECL Plus Western blotting detection system (GE Healthcare, Buckinghamshire, UK).

Supporting Information

Figure S1 ATP Levels in HCV replicon cells and parental Huh-7 cells determined by CE-TOF MS. ATP metabolites in Huh-7 cells and JFH-1/4-5 cells were measured by

CE-TOFMS. The values of each measurement are shown at left. The right graph shows means with SD of the data at left. Open bar; Huh-7 cells, gray bar; JFH-1/4-5 cells.
(TIF)

Figure S2 Cytoplasmic ATP levels in HCV replicon cells and IFN-treated cells. (Left) The HCV replicon cells JFH-1/4-1, JFH-1/4-5 (genotype 2a) and NK5.1/0-9 (genotype 1b), and parental Huh-7 cells were cultured for 72 h in the absence or presence of 1,000 IU/ml IFN-alpha. Forty-eight hours after transfection with AT1.03, the Venus/CFP emission ratio of each cell was calculated from fluorescent images acquired with the confocal microscope FV1000. All data are presented as means and SD for at least 10 independent cells. (Right) HCV RNA titers in cells corresponding to the left panel were determined using real-time quantitative RT-PCR. Data are presented as means and SD for three independent samples. NTD indicates not detected.
(TIF)

Figure S3 Increase in ATP-enriched dot-like structures in cells replicating SGR-ATeam. Huh-7 cells were transfected with SGR-AT1.03, and analyzed in the same way as described in the legends for Figures 5A and 5B. The lower four panels are five-fold magnifications of the boxed areas in independent cells. Scale bars, 40 μm.
(TIF)

Figure S4 Visualization of the ATP level in cells expressing replication-defective HCV polyprotein. (A) A schematic representation of the NS3-NS5B-AT1.03 plasmid is shown. The HCV polyprotein is indicated by the open boxes. The ATeam gene was inserted into the same site as that for NS5A-ATeam and SGR-ATeam insertion as indicated in the legend for Figure 4A. CAG, CAG promoter. (B) Cells transfected with constructs encoding NS5A, NS5A-AT1.03, NS3-NS5B-AT1.03, SGR or SGR-AT1.03 were analyzed by immunoblotting with anti-NS5A, anti-NS5B or anti-beta-actin antibodies. (C) Huh-7 cells were transfected with NS3-NS5B-AT1.03, and analyzed in the same way as described in the legends for Figures 5A and 5B. The upper panel (Fluorescence) demonstrates signal intensity from a spectral channel with maximum intensity and represents the expression pattern of NS5A-ATeam processed from NS3-NS5B-AT1.03. The lower panels (Venus/CFP ratio) indicate the FRET ratio and a five-fold magnification of the boxed area. Scale bar, 20 μm.
(TIF)

Figure S5 Relationship between ATP-enriched dot-like structures and mitochondria. Huh-7 cells replicating SGR-AT1.03 (right panels) and parental cells (left panel) were analyzed. Active mitochondria were labeled with MitoTracker Red CMXRos in living cells, and were analyzed in the same way as described in the legends for Figures 5A and 5B, using a reference for the MitoTracker spectrum. The lowest panels of SGR-ATeam cells indicate five-fold magnifications of the boxed areas. Scale bars, 20 μm.
(TIF)

Figure S6 Inhibitory effect of PSI-6130 on HCV RNA replication. (A) Replication levels of SGR/luc-AT1.03 RNA in transfected cells were determined by luciferase assay 3 days after treatment with PSI-6130 at the indicated concentrations (μM). The values shown were normalized for transfection efficiency with luciferase activity determined 24 h post-transfection. All data are presented as means and SD for three independent samples. (B) Cell viability was assessed using the MTT assay.
(TIF)

Acknowledgments

We are grateful to Minoru Tobiume, Tadaki Suzuki, Teruyuki Nagamune, Satoshi Yamaguchi, Yoshiharu Matsuura, Hiroto Kambara, Tomoko Date, Su Su Hmwe, Koichi Watashi, Takahiro Masaki and Takanobu Kato for their excellent technical assistance and advice, as well as to Takeharu Nagai for providing the mVenus expression vector and to Atsushi Miyawaki for providing the mseCFP expression vector. We thank our coworkers for their helpful discussions. We also thank Mami Sasaki for her technical assistance and Tomoko Mizoguchi for her secretarial work. We also thank the University of Tokyo Center for NanoBio Integration and the Department of Pathology in the National Institute of Infectious Diseases, Japan, for use of their confocal microscope.

Author Contributions

Conceived and designed the experiments: T. Ando, H. Imamura, T. Wakita, T. Suzuki. Performed the experiments: T. Ando, H. Aizaki. Analyzed the data: T. Ando, H. Imamura, T. Watanabe, T. Wakita, T. Suzuki. Contributed reagents/materials/analysis tools: H. Imamura, R. Suzuki, H. Aizaki. Wrote the paper: T. Ando, T. Suzuki.

References

1. Ranji A, Boris-Lawrie K (2010) RNA helicases: Emerging roles in viral replication and the host innate response. RNA Biol 7: 775–787.
2. Imamura H, Nhat KP, Togawa H, Saito K, Iino R, et al. (2009) Visualization of ATP levels inside single living cells with fluorescence resonance energy transfer-based genetically encoded indicators. Proc Natl Acad Sci U S A 106: 15651–15656.
3. Kato-Yamada Y, Yoshida M (2003) Isolated epsilon subunit of thermophilic F1-ATPase binds ATP. J Biol Chem 278: 36013–36016.
4. Iino R, Murakami T, Iizuka S, Kato-Yamada Y, Suzuki T, et al. (2005) Real-time monitoring of conformational dynamics of the epsilon subunit in F1-ATPase. J Biol Chem 280: 40130–40134.
5. Yagi H, Kajiwara N, Tanaka H, Tsukihara T, Kato-Yamada Y, et al. (2007) Structures of the thermophilic F1-ATPase epsilon subunit suggesting ATP-regulated arm motion of its C-terminal domain in F1. Proc Natl Acad Sci U S A 104: 11233–11238.
6. Bartenschlager R, Sparacio S (2007) Hepatitis C virus molecular clones and their replication capacity in vivo and in cell culture. Virus Res 127: 195–207.
7. Pezacki JP, Singaravelu R, Lyn RK (2010) Host-virus interactions during hepatitis C virus infection: a complex and dynamic molecular biosystem. Mol Biosyst 6: 1131–1142.
8. Suzuki T, Ishii K, Aizaki H, Wakita T (2007) Hepatitis C viral life cycle. Adv Drug Deliv Rev 59: 1200–1212.
9. Cai Z, Liang TJ, Luo G (2004) Effects of Mutations of the Initiation Nucleotides on Hepatitis C Virus RNA Replication in the Cell. J Virol 78: 3633–3643.
10. Moradpour D, Penin F, Rice CM (2007) Replication of hepatitis C virus. Nat Rev Microbiol 5: 453–463.
11. Dumont S, Cheng W, Serebrov V, Beran RK, Tinoco I, Jr., et al. (2006) RNA translocation and unwinding mechanism of HCV NS3 helicase and its coordination by ATP. Nature 439: 105–108.
12. Frick DN (2007) The hepatitis C virus NS3 protein: a model RNA helicase and potential drug target. Curr Issues Mol Biol 9: 1–20.
13. Miyanari Y, Hijikata M, Yamaji M, Hosaka M, Takahashi H, et al. (2003) Hepatitis C virus non-structural proteins in the probable membranous compartment function in viral genome replication. J Biol Chem 278: 50301–50308.
14. Wakita T, Pietschmann T, Kato T, Date T, Miyamoto M, et al. (2005) Production of infectious hepatitis C virus in tissue culture from a cloned viral genome. Nat Med 11: 791–796.
15. Miyamoto M, Kato T, Date T, Mizokami M, Wakita T (2006) Comparison between subgenomic replicons of hepatitis C virus genotypes 2a (JFH-1) and 1b (Con1 NK5.1). Intervirology 49: 37–43.
16. Mankouri J, Tedbury PR, Gretton S, Hughes ME, Griffin SD, et al. (2010) Enhanced hepatitis C virus genome replication and lipid accumulation mediated by inhibition of AMP-activated protein kinase. Proc Natl Acad Sci U S A 107: 11549–11554.
17. Nakashima K, Takeuchi K, Chihara K, Hotta H, Sada K (2011) Inhibition of hepatitis C virus replication through adenosine monophosphate-activated protein kinase-dependent and -independent pathways. Microbiol Immunol 55: 774–782.

18. Nagai T, Ibata K, Park ES, Kubota M, Mikoshiba K, et al. (2002) A variant of yellow fluorescent protein with fast and efficient maturation for cell-biological applications. Nat Biotechnol 20: 87–90.
19. Appleby TC, Anderson R, Fedorova O, Pyle AM, Wang R, et al. (2011) Visualizing ATP-dependent RNA translocation by the NS3 helicase from HCV. J Mol Biol 405: 1139–1153.
20. Cheng W, Arunajadai SG, Moffitt JR, Tinoco I, Jr., Bustamante C (2011) Single-base pair unwinding and asynchronous RNA release by the hepatitis C virus NS3 helicase. Science 333: 1746–1749.
21. Beran RK, Lindenbach BD, Pyle AM (2009) The NS4A protein of hepatitis C virus promotes RNA-coupled ATP hydrolysis by the NS3 helicase. J Virol 83: 3268–3275.
22. Hara H, Aizaki H, Matsuda M, Shinkai-Ouchi F, Inoue Y, et al. (2009) Involvement of creatine kinase B in hepatitis C virus genome replication through interaction with the viral NS4A protein. J Virol 83: 5137–5147.
23. Ma H, Jiang WR, Robledo N, Leveque V, Ali S, et al. (2007) Characterization of the metabolic activation of hepatitis C virus nucleoside inhibitor beta-D-2′-Deoxy-2′-fluoro-2′-C-methylcytidine (PSI-6130) and identification of a novel active 5′-triphosphate species. J Biol Chem 282: 29812–29820.
24. Murakami E, Bao H, Ramesh M, McBrayer TR, Whitaker T, et al. (2007) Mechanism of activation of beta-D-2′-deoxy-2′-fluoro-2′-c-methylcytidine and inhibition of hepatitis C virus NS5B RNA polymerase. Antimicrob Agents Chemother 51: 503–509.
25. Moradpour D, Evans MJ, Gosert R, Yuan Z, Blum HE, et al. (2004) Insertion of green fluorescent protein into nonstructural protein 5A allows direct visualization of functional hepatitis C virus replication complexes. J Virol 78: 7400–7409.
26. Masaki T, Suzuki R, Saeed M, Mori K, Matsuda M, et al. (2010) Production of infectious hepatitis C virus by using RNA polymerase I-mediated transcription. J Virol 84: 5824–5835.
27. Shi ST, Lee KJ, Aizaki H, Hwang SB, Lai MMC (2003) Hepatitis C Virus RNA Replication Occurs on a Detergent-Resistant Membrane That Cofractionates with Caveolin-2. J Virol 77: 4160–4168.
28. Gosert R, Egger D, Lohmann V, Bartenschlager R, Blum HE, et al. (2003) Identification of the Hepatitis C Virus RNA Replication Complex in Huh-7 Cells Harboring Subgenomic Replicons. J Virol 77: 5487–5492.
29. Palmer AE, Jin C, Reed JC, Tsien RY (2004) Bcl-2-mediated alterations in endoplasmic reticulum Ca2+ analyzed with an improved genetically encoded fluorescent sensor. Proc Natl Acad Sci U S A 101: 17404–17409.
30. Dittmer PJ, Miranda JG, Gorski JA, Palmer AE (2009) Genetically encoded sensors to elucidate spatial distribution of cellular zinc. J Biol Chem 284: 16289–16297.
31. Nomaguchi M, Ackermann M, Yon C, You S, Padmanbhan R (2003) De Novo Synthesis of Negative-Strand RNA by Dengue Virus RNA-Dependent RNA Polymerase In Vitro: Nucleotide, Primer, and Template Parameters. J Virol 77: 8831–8842.
32. Klumpp K, Ford MJ, Ruigrok RW (1998) Variation in ATP requirement during influenza virus transcription. J Gen Virol 79(Pt 5): 1033–1045.
33. Vreede FT, Gifford H, Brownlee GG (2008) Role of initiating nucleoside triphosphate concentrations in the regulation of influenza virus replication and transcription. J Virol 82: 6902–6910.
34. Frick DN, Lam AM (2006) Understanding helicases as a means of virus control. Curr Pharm Des 12: 1315–1338.
35. Gurer C, Hoglund A, Hoglund S, Luban J (2005) ATPgammaS disrupts human immunodeficiency virus type 1 virion core integrity. J Virol 79: 5557–5567.
36. Li PP, Itoh N, Watanabe M, Shi Y, Liu P, et al. (2009) Association of simian virus 40 vp1 with 70-kilodalton heat shock proteins and viral tumor antigens. J Virol 83: 37–46.
37. Dennis PB, Jaeschke A, Saitoh M, Fowler B, Kozma SC, et al. (2001) Mammalian TOR: a homeostatic ATP sensor. Science 294: 1102–1105.
38. Zamaraeva MV, Sabirov RZ, Maeno E, Ando-Akatsuka Y, Bessonova SV, et al. (2005) Cells die with increased cytosolic ATP during apoptosis: a bioluminescence study with intracellular luciferase. Cell Death Differ 12: 1390–1397.
39. Berg J, Hung YP, Yellen G (2009) A genetically encoded fluorescent reporter of ATP:ADP ratio. Nat Methods 6: 161–166.
40. Niwa H, Yamamura K, Miyazaki J (1991) Efficient selection for high-expression transfectants with a novel eukaryotic vector. Gene 108: 193–199.
41. Soga T, Ohashi,Y, Ueno Y, Naraoka H, Tomita M, et al. (2003) Quantitative metabolome analysis using capillary electrophoresis mass spectrometry. J Proteome Res 2: 488–494.
42. Haraguchi T, Shimi T, Koujin T, Hashiguchi N, Hiraoka Y (2002) Spectral imaging fluorescence microscopy. Genes Cells 7: 881–887.
43. Ishii M, Ikushima M, Kurachi Y (2005) In vivo interaction between RGS4 and calmodulin visualized with FRET techniques: possible involvement of lipid raft. Biochem Biophys Res Commun 338: 839–846.
44. Murakami K, Kimura T, Osaki M, Ishii K, Miyamura T, et al. (2008) Virological characterization of the hepatitis C virus JFH-1 strain in lymphocytic cell lines. J Gen Virol 89: 1587–1592.
45. Inoue Y, Aizaki H, Hara H, Matsuda M, Ando T, et al. (2011) Chaperonin TRiC/CCT participates in replication of hepatitis C virus genome via interaction with the viral NS5B protein. Virology 410: 38–47.
46. Taguwa S, Kambara H, Omori H, Tani H, Abe T, et al. (2009) Cochaperone activity of human butyrate-induced transcript 1 facilitates hepatitis C virus replication through an Hsp90-dependent pathway. J Virol 83: 10427–10436.
47. Takeuchi T, Katsume A, Tanaka T, Abe A, Inoue K, et al. (1999) Real-time detection system for quantification of hepatitis C virus genome. Gastroenterology 116: 636–642.

Incorporation of Biaryl Units into the 5′ and 3′ Ends of Sense and Antisense Strands of siRNA Duplexes Improves Strand Selectivity and Nuclease Resistance

Kayo Yoshikawa,[†] Aya Ogata,[†] Chiho Matsuda,[§] Michinori Kohara,[§] Hideo Iba,[||] Yukio Kitade,[†,‡] and Yoshihito Ueno*[,†,‡]

Department of Biomolecular Science, Faculty of Engineering, and United Graduate School of Drug Discovery and Medical Information Sciences, Gifu University, 1-1 Yanagido, Gifu 501-1193, Japan, Department of Microbiology and Cell Biology, The Tokyo Metropolitan Institute of Medical Science, 2-1-6, Kamikitazawa, Setagaya-ku, Tokyo 156-0057, Japan, and Division of Host-Parasite Interaction, Department of Microbiology and Immunology, Institute of Medical Science, The University of Tokyo, 4-6-1 Shirokanedai, Minato-ku, Tokyo 108-8639, Japan. Received July 5, 2010; Revised Manuscript Received November 30, 2010

Small interfering RNA (siRNA) is a noncoding RNA with considerable potential as a new therapeutic drug for intractable diseases. siRNAs can be rationally designed and synthesized if the sequences of the disease-causing genes are known. In this paper, we describe the synthesis and properties of siRNAs modified with biaryl units. We found that incorporation of biaryl units into the 5′ and 3′ ends of sense and antisense strands of siRNA duplexes improved strand selectivity and nuclease resistance.

INTRODUCTION

RNA interference (RNAi) is a biological process whereby double-stranded RNAs (dsRNAs) silence gene expression in a sequence-specific manner (*1*). Small RNAs, including small interfering RNA (siRNA) and microRNA (miRNA), are key intermediates in RNAi. They regulate gene expression through the RNA-induced silencing complex (RISC), which contains Argonaute proteins as core components. siRNAs hold considerable potential as new therapeutic drugs for intractable diseases, because they can be rationally designed and synthesized if the sequences of disease-causing genes are known (*2*−*6*).

One strand from an siRNA or miRNA duplex is selected and loaded onto RISC to become mature siRNA or miRNA. It has been suggested that RISC preferentially selects and incorporates one of two strands of the siRNA duplex, depending on its thermodynamic features. The strand with thermodynamically lower stability in its 5′-terminus (the guide strand) preferentially binds the RISC and becomes functional, whereas the other strand (the passenger strand) is degraded (*7*−*9*). However, it has recently become clear that strand selection does not always follow this rule (*1*−*14*). Recently reported siRNA studies demonstrated that modifying the 5′-terminus of one strand with 5′-*O*-methyl efficiently specifies its antisense strand to be loaded onto RISC despite thermodynamic disadvantages (*15*), because 5′-*O*-methyl inhibits phosphorylation of the 5′-terminus, which is an important factor for RISC loading (*16*−*20*).

We have reported the synthesis of DNAs containing biaryl units, **3** and **5**, which comprised benzene and naphthalene or pyrene residues (Figure 1). The biaryl units thermally and thermodynamically stabilized DNA/DNA duplexes (*21*). We have also succeeded in improving siRNA nuclease resistance by introduction of bis(hydroxymethyl)benzene (**1**) instead of thymidine at 3′-overhangs without reducing RNAi-inducing activity (*22*). From these results and background information, we planned the synthesis of siRNAs with biaryl units at the 5′ and 3′ ends of sense and antisense strands of siRNA duplexes, respectively. We expected that thermal and thermodynamic stabilities of the 5′ regions of siRNA sense strands would be increased by these biaryl modifications. Phosphorylation of the 5′ ends of sense strands, an important factor for RISC loading, was expected to be inhibited by biaryl protection of 5′-hydroxyls. We anticipated that these modifications would enhance RISC loading of antisense strands of siRNA duplexes, suppressing off-target effects induced by sense strands. We also anticipated improved nuclease resistance in biaryl-modified siRNAs, which is important for the therapeutic application of synthetic siRNAs.

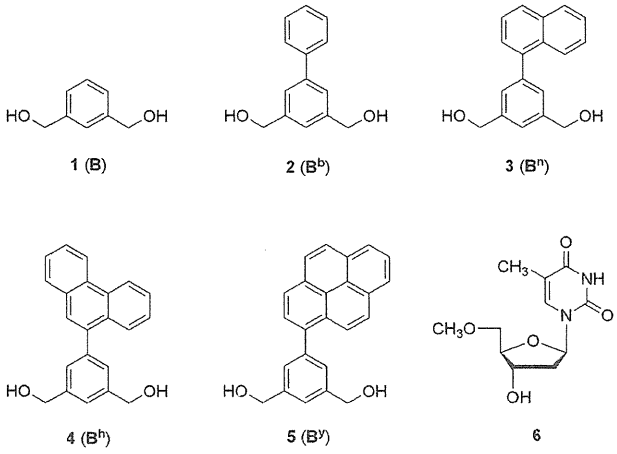

Figure 1. Structures of the aromatic compounds and modified nucleoside used in this study.

In this paper, we report the synthesis and properties of siRNA duplexes which carry biaryl units at the 5′ and 3′ ends of sense and antisense strands, respectively. We assessed the gene

* To whom correspondence should be addressed. Phone: +81-58-293-2639. Fax: +81-58-293-2794. E-mail: uenoy@gifu-u.ac.jp.
[†] Department of Biomolecular Science, Faculty of Engineering, Gifu University.
[‡] United Graduate School of Drug Discovery and Medical Information Sciences, Gifu University.
[§] The Tokyo Metropolitan Institute of Medical Science.
[||] The University of Tokyo.

10.1021/bc100301w
Published on Web 12/09/2010

Scheme 1[a]

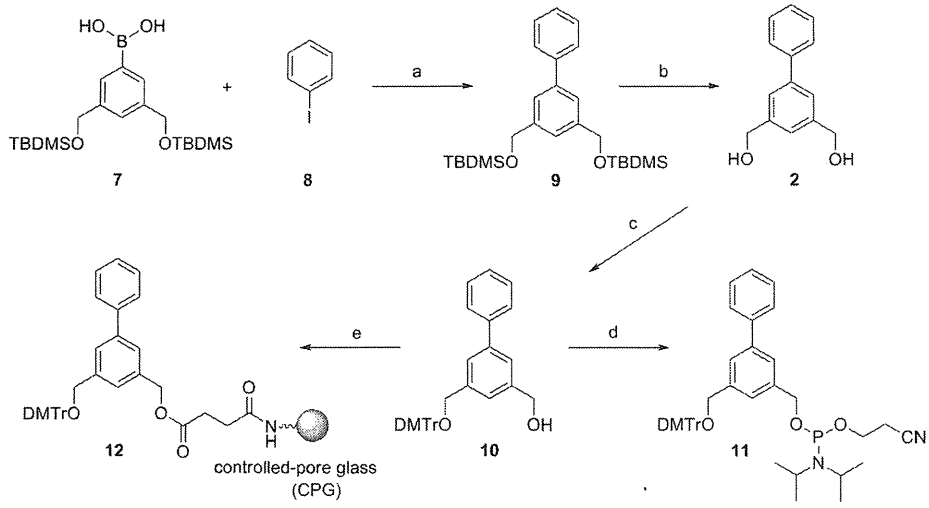

[a] Reagents and conditions: (a) $PdCl_2(dppf)\cdot CH_2Cl_2$, NaOH, THF/$H_2O$ (5:1 v/v), 65 °C, 24 h; (b) TBAF, THF, rt, 2 h, 93% from **7**; (c) DMTrCl, pyridine, rt, 4 h, 52%; (d) chloro(2-cyanoethoxy)(*N*,*N*-diisopropylamino)phosphane, *i*-Pr_2NEt, THF, rt, 1 h, 88%; (e) (1) succinic anhydride, DMAP, pyridine, rt, 24 h; (2) CPG, EDCI, DMF, rt, 48 h, 49 μmol/g loading amount.

Scheme 2[a]

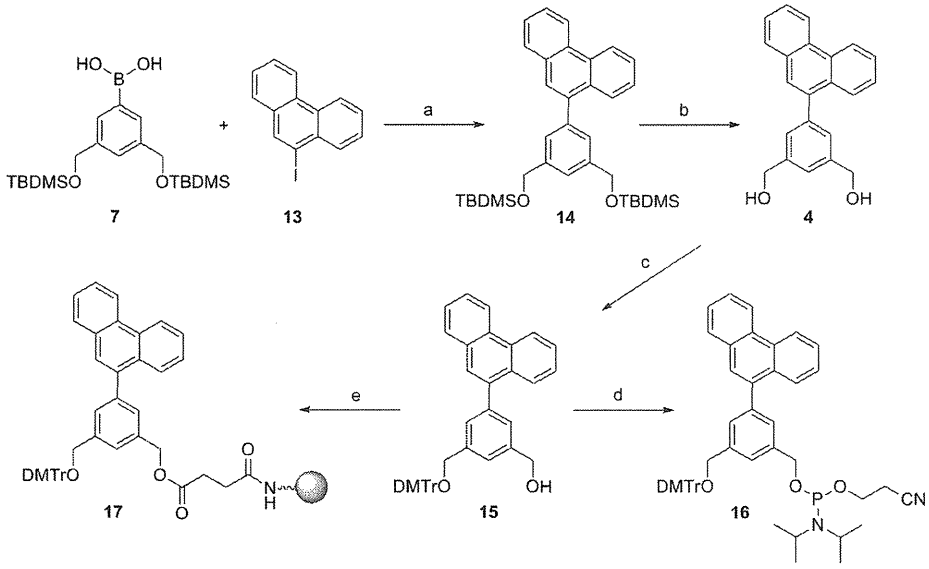

[a] Reagents and conditions: (a) $PdCl_2(dppf)\cdot CH_2Cl_2$, NaOH, THF/$H_2O$ (5:1 v/v), 65 °C, 24 h; (b) TBAF, THF, rt, 2 h, 60% from **7**; (c) DMTrCl, pyridine, rt, 3 h, 61%; (d) chloro(2-cyanoethoxy)(*N*,*N*-diisopropylamino)phosphane, *i*-Pr_2NEt, THF, rt, 1 h, 74%; (e) (1) succinic anhydride, DMAP, pyridine, rt, 24 h; (2) CPG, EDCI, DMF, rt, 48 h, 45 μmol/g loading amount.

silencing activities of the modified siRNAs by a dual-luciferase assay. We also assessed the nuclease-resistance of the modified siRNAs.

RESULTS AND DISCUSSION

Design and Synthesis of siRNAs. The Argonaute proteins are core components of RISC, which is responsible for mRNA cleavage in the RNAi pathway. The proteins are composed of PAZ, Mid, and PIWI domains. X-ray structural analysis and a nuclear magnetic resonance (NMR) study have revealed that the 3′-overhang region of a guide strand of siRNA is recognized by the PAZ domain and the 2-nucleotide (nt) 3′-overhang is accommodated by a binding pocket composed of hydrophobic amino acids (*23*−*26*). In order to estimate the appropriate size for biaryl units in the 3′-overhang region, we assessed the silencing activities of siRNAs which carried various types of biaryl units at the 3′-overhangs.

We assessed the biaryl units **2** (B^b), **3** (B^a), **4** (B^h), and **5** (B^y), comprising benzene and benzene, naphthalene, phenanthrene, or pyrene residues, to determine the appropriate size for the 3′-overhang regions. Phosphoramidites of **3** and **5** were synthesized according to a previously reported method (*21*). Phosphoramidites of **2** and **4** and solid supports carrying **2** or **4** were synthesized according to the methods shown in Schemes 1 and 2. An arylboronic acid derivative **7** was coupled with iodobenzene (**8**) in the presence of $PdCl_2(dppf)$ (dppf stands for 1,1′-bis(diphenylphosphanyl)ferrocene) at 65 °C; this coupling reaction produced the biaryl derivative **9**; subsequently, **9** was desilylated by treatment with tetra-*n*-butylammonium fluoride (TBAF) to give a 93% yield of biaryl unit **2**. One out of the two hydroxy groups of **2** was protected by a 4,4′-dimethoxytrityl (DMTr) group to give a 52% yield of mono-DMTr derivative **10**. **10** was phosphitylated by the standard procedure to produce the corresponding phosphoramidite **11** at

Table 1. Sequences of ONs and siRNAs[a]

no. of siRNA	no. of ON	sequence
siRNA**18**	ON**43**	5′-GGCCUUUCACUACUCCUAC*tt*-3′
	ON**44**	3′-*tt*CCGGAAAGUGAUGAGGAUG-5′
siRNA**19**	ON**45**	5′-GGCCUUUCACUACUCCUAC**B^{b}B^b**-3′
	ON**46**	3′-**B^{b}B^b**CCGGAAAGUGAUGAGGAUG-5′
siRNA**20**	ON**47**	5′-GGCCUUUCACUACUCCUAC**B^{n}B^n**-3′
	ON**48**	3′-**B^{n}B^n**CCGGAAAGUGAUGAGGAUG-5′
siRNA**21**	ON**49**	5′-GGCCUUUCACUACUCCUAC**B^{h}B^h**-3′
	ON**50**	3′-**B^{h}B^h**CCGGAAAGUGAUGAGGAUG-5′
siRNA**22**	ON**51**	5′-GGCCUUUCACUACUCCUAC**B^{y}B^y**-3′
	ON**52**	3′-**B^{y}B^y**CCGGAAAGUGAUGAGGAUG-5′
siRNA**23**	ON**53**	**F**-5′-GGCCUUUCACUACUCCUAC*tt*-3′
	ON**44**	3′-*tt*CCGGAAAGUGAUGAGGAUG-5′
siRNA**24**	ON**54**	**F**-5′-GGCCUUUCACUACUCCUAC**B^{b}B^b**-3′
	ON**46**	3′-**B^{b}B^b**CCGGAAAGUGAUGAGGAUG-5′
siRNA**25**	ON**55**	5′-CUUCUUCGUCGAGACCAUG*tt*-3′
	ON**56**	3′-*tt*GAAGAAGCAGCUCUGGUAC-5′
siRNA**26**	ON**57**	5′-**B^b**CUUCUUCGUCGAGACCAUG*tt*-3′
	ON**56**	3′-*tt*GAAGAAGCAGCUCUGGUAC-5′
siRNA**27**	ON**58**	5′-**B^n**CUUCUUCGUCGAGACCAUG*tt*-3′
	ON**56**	3′-*tt*GAAGAAGCAGCUCUGGUAC-5′
siRNA**28**	ON**55**	5′-CUUCUUCGUCGAGACCAUG*tt*-3′
	ON**59**	3′-*tt*GAAGAAGCAGCUCUGGUAC**B^b**-5′
siRNA**29**	ON**55**	5′-CUUCUUCGUCGAGACCAUG*tt*-3′
	ON**60**	3′-*tt*GAAGAAGCAGCUCUGGUAC**B^n**-5′
siRNA**30**	ON**61**	5′-UUUCACUACUCCUACGAGC*tt*-3′
	ON**62**	3′-*tt*AAAGUGAUGAGGAUGCUCG-5′
siRNA**31**	ON**63**	5′-**B^n**UUUCACUACUCCUACGAGC**BB**-3′
	ON**64**	3′-**BB^n**AAAGUGAUGAGGAUGCUCG-5′
siRNA**32**	ON**63**	5′-**B^n**UUUCACUACUCCUACGAGC**BB**-3′
	ON**65**	3′-**B^{n}B^n**AAAGUGAUGAGGAUGCUCG-5′
siRNA**33**	ON**66**	5′-**T^m**UUCACUACUCCUACGAGC*tt*-3′
	ON**62**	3′-*tt*AAAGUGAUGAGGAUGCUCG-5′
siRNA**34**	ON**67**	5′-UAAGAUGUUCAUCGAGUCC*tt*-3′
	ON**68**	3′-*tt*AUUCUACAAGUAGCUCAGG-5′
siRNA**35**	ON**69**	5′-**B^n**UAAGAUGUUCAUCGAGUCC**BB**-3′
	ON**70**	3′-**BB^n**AUUCUACAAGUAGCUCAGG-5′
siRNA**36**	ON**69**	5′-**B^n**UAAGAUGUUCAUCGAGUCC**BB**-3′
	ON**71**	3′-**B^{n}B^n**AUUCUACAAGUAGCUCAGG-5′
siRNA**37**	ON**72**	5′-GUCUCGUAGACCGUGCAUCA*tt*-3′
	ON**73**	3′-*tt*CAGAGCAUCUGGCACGUAGU-5′
siRNA**38**	ON**74**	5′-GUCUCGUAGACCGUGCAUCA**BB**-3′
	ON**75**	3′-**BB**CAGAGCAUCUGGCACGUAGU-5′
siRNA**39**	ON**76**	5′-**B^n**GUCUCGUAGACCGUGCAUCA**BB**-3′
	ON**77**	3′-**BB^n**CAGAGCAUCUGGCACGUAGU-5′
siRNA**40**	ON**76**	5′-**B^n**GUCUCGUAGACCGUGCAUCA**BB**-3′
	ON**75**	3′-**BB**CAGAGCAUCUGGCACGUAGU-5′
siRNA**41**	ON**74**	5′-GUCUCGUAGACCGUGCAUCA**BB**-3′
	ON**77**	3′-**BB^n**CAGAGCAUCUGGCACGUAGU-5′
siRNA**42**	ON**78**	5′-**B^n**GUCUCAUAGGCCAUGCGUCA**BB**-3′
	ON**79**	3′-**BB^n**CAGAGUAUCCGGUACGCAGU-5′

[a] The small italic letters represent 2′-deoxyribonucleosides. The underlined letters indicate mismatched bases. **F** shows fluorescein.

an 88% yield. In a similar manner, phosphoramidite **16** was synthesized from 9-iodophenanthrene (**13**); the total yield of **16** was 27%.

To enable attachment to the solid support, the mono-DMTr derivative **10** was succinated to yield the corresponding succinate, which was linked to controlled pore glass (CPG) to create the solid support **12** linked to **10** (49 μmol/g). Similarly, the mono-DMTr derivative **15** was succinated and linked to the CPGs to yield the solid supports **17** linked to **15** (45 μmol/g). siRNA sequences used in this study are depicted in Table 1.

Thermal Denaturation Study of siRNAs. Thermal stability of biaryl-modified siRNAs was studied by thermal denaturation in 0.01 M sodium phosphate buffer (pH 7.0) containing 0.1 M NaCl (Table 2). The melting temperature (T_ms) of unmodified siRNA**18** was 79.1 °C, while those of siRNAs **19**, **20**, **21**, and **22** were 77.9, 80.7, 82.2, and 82.8 °C, respectively. The siRNA duplexes were found to become more thermostable with increasing biaryl unit size. This result suggests that thermal

Table 2. T_m Values[a]

no. of siRNA	T_m (°C)	ΔT_m (°C)
siRNA**18**	79.1	
siRNA**19**	79.9	+0.8
siRNA**20**	80.7	+1.6
siRNA**21**	82.2	+3.1
siRNA**22**	82.8	+3.7

[a] The experimental conditions are as described in the Experimental Section.

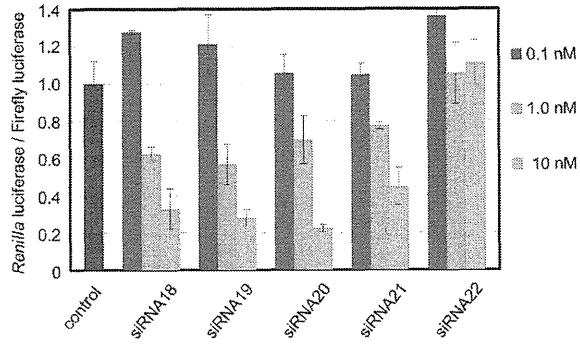

Figure 2. Dual-luciferase assay (1). The experimental conditions are as described in the Experimental Section.

stabilization of the duplexes is attributable to stacking interactions of the biaryl units with adjacent nucleotides.

Dual-Luciferase Assay. We assessed the silencing activity of modified siRNAs by performing a dual-luciferase assay using the psiCHECK-2 vector. siRNA sequences were designed to target *Renilla* luciferase. Reporter vectors and synthesized siRNA duplexes were cotransfected into HeLa cells, and luciferase activities were measured after 24 h. The signals of *Renilla* luciferase were normalized to those of firefly luciferase.

As shown in Figure 2, siRNA**18**, **19**, and **20**, which carried natural thymidines, **B^b**s or **B^n**s at their 3′-overhangs, effectively reduced luciferase activity in a dose-dependent manner. In contrast, the silencing activity of siRNA**21**, which contained **B^h** comprising a tricyclic phenanthrene residue, was apparently weaker than that of unmodified siRNA**18**. Further, siRNA**22**, which carried **B^y** with a tetracyclic pyrene residue, had no silencing activity. Thus, biaryl units smaller than the naphthalene type are acceptable for the 3′-overhang region of siRNAs. These results are consistent with a recent report from Somoza et al (*27*).

Microarray profiling studies have demonstrated that siRNAs may silence multiple genes in addition to the intended target (*28, 29*). This unintended (off-target) transcript silencing is a critical problem associated with RNAi-based therapeutic applications. Both the sense and antisense strands of an siRNA can contribute to the off-target effects. Thus, to minimize the extent of sense-strand incorporation into an activated RISC, we next examined the silencing activity of siRNAs, which involved the biaryl units at the 5′ ends of sense or antisense strands of siRNA duplexes. We expected that inhibition of 5′-*O*-phosphorylation of sense strands with biaryl protection of 5′-hydroxyls would enhance RISC loading of antisense strands.

Figure 3a shows the results of siRNAs modified at the 5′ ends of sense strands with biaryl units **B^b** and **B^n**, whereas Figure 3b represents those modified at the 5′ ends of antisense strands. Modifications at the 5′ ends of sense strands did not influence siRNA silencing activity, whereas modifications at the 5′ ends of antisense strands markedly reduced silencing activity. Thus, it was found that the biaryl modifications at the 5′-termini of the sense strands could induce the antisense strand specificity of the siRNA duplexes.

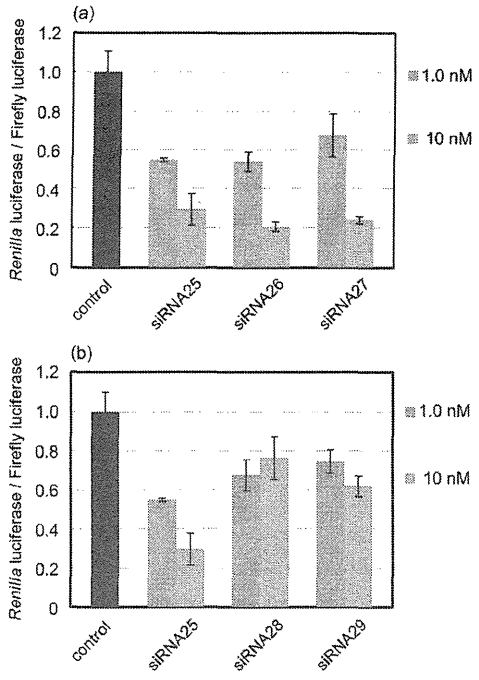

Figure 3. Dual-luciferase assay (2). (a) siRNAs modified at 5′-ends of passenger (sense) strands. (b) siRNAs modified at 5′-ends of guide (antisense) strands.

Next, we designed siRNAs which carried biaryl units at the 5′ and 3′ ends of sense and antisense strands, respectively. We speculated that incorporation of the biaryl units into the 5′ and 3′ ends of sense and antisense strands of siRNAs would increase the thermal and thermodynamic stabilities of the sense-strand 5′ siRNA regions. Further, introduction of the biaryl units at the 5′ ends of sense strands would inhibit phosphorylation, which is an important factor for RISC loading. We hypothesized that these modifications would work synergistically, creating more potent siRNAs.

We selected target sequences containing high frequencies of U and A bases, which are thought to be unsuitable targets for siRNA (Table 1). The results of dual-luciferase assays are shown in Figure 4a and b. Unmodified siRNA**30** exhibited almost no silencing activity, whereas siRNA**31** and **32** modified with **B** and **B**^{n} reduced luciferase activity in a dose-dependent manner (Figure 4a). Silencing activities of biaryl-modified siRNA**31** and **32** were greater than that of siRNA**33** containing 5′-*O*-methylthymidine at the 5′ end of the sense strand at all concentrations. This indicates that not only inhibition of phosphorylation, but also thermal stabilization of the 5′ regions of sense strands, contributes to improving siRNA silencing activity. Similarly, unmodified siRNA**34** had almost no silencing activity, whereas biaryl-modified siRNA**35** and **36** efficiently suppressed luciferase expression in a dose-dependent manner (Figure 4b). These results suggest that biaryl modification may provide a good method for improving siRNA silencing activities of sequences which are thought to be unsuitable siRNA targets.

Nuclease Resistance. Improving the nuclease resistance of siRNA is important for the therapeutic application of synthetic siRNAs. It was expected that biaryl-modified RNAs would be more nuclease resistant than unmodified RNAs. First, the susceptibility of the ONs to snake venom phosphodiesterase (SVPD), a 3′-exonuclease, was examined. Unmodified ON**53** and modified ON**54**, which were labeled at the 5′-ends with fluorescein, were incubated with SVPD. The reactions were analyzed using PAGE under denaturing conditions. As shown in Figure 5a, unmodified ON**53** was hydrolyzed randomly after

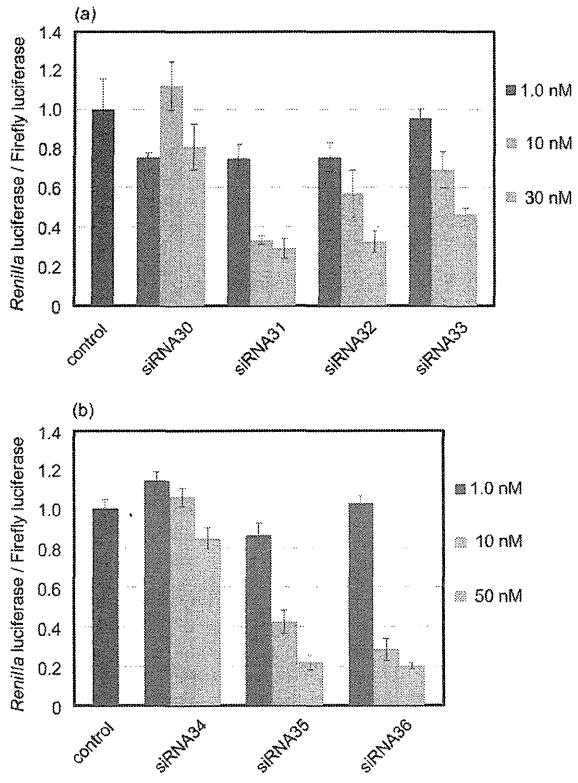

Figure 4. Dual-luciferase assay (3). The experimental conditions are as given in the Experimental Section.

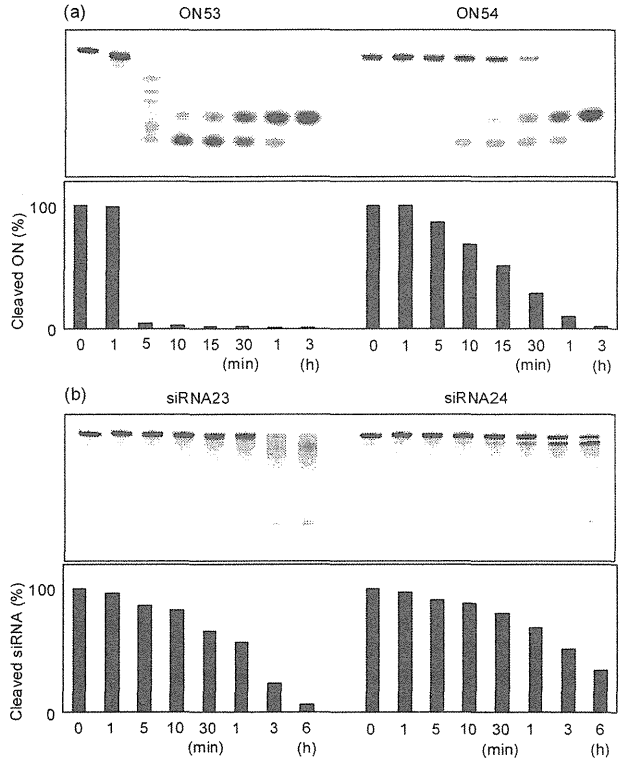

Figure 5. (a) 20% PAGE of 5′-fluorescein-labeled ONs hydrolyzed by SVPD. (b) 20% PAGE of 5′-fluorescein-labeled siRNAs incubated in PBS containing 40% bovine serum. The experimental conditions are as described in the Experimental Section.

5 min of incubation, while modified ON**54** was resistant to the enzyme. The half-life ($t_{1/2}$) of unmodified ON**53** was less than

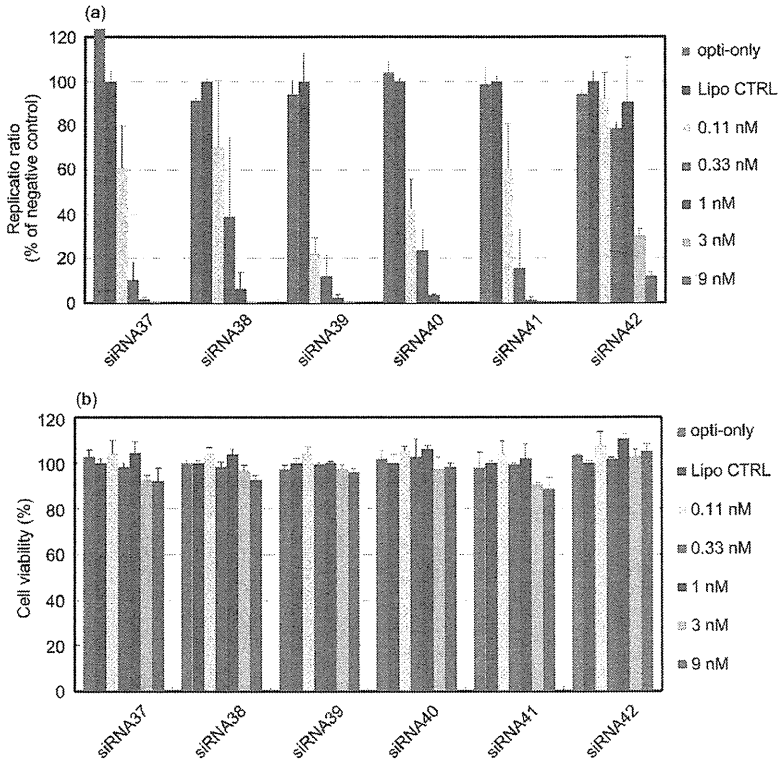

Figure 6. Effect of siRNAs on HCV replication. (a) Inhibition of HCV replication by siRNAs in R6FLR-N replicon cells. HCV replication was calculated by measuring the luminescence ratio with a Bright-Glo luciferase assay system. (b) Cell viability was determined by a WST-8 assay. Data are represented as mean (SD) (n = 3). The experimental conditions are as described in the Experimental Section.

5 min, whereas that of the modified ON**54** was 17 min. ON**54** carrying $\mathbf{B}^{\mathbf{b}}$ at its 3′-end was significantly more resistant to SVPD than unmodified ON**53**.

Next, the stability of siRNAs in PBS containing bovine serum was investigated. Unmodified siRNA**23** and modified siRNA**24**, which were fluorescein-labeled at the 5′ ends of sense strands, were incubated in PBS containing 40% bovine serum. The reactions were analyzed with PAGE under nondenaturing conditions. Figure 5b shows the results. After 6 h of incubation, the band corresponding to the modified siRNA**24** duplex was observed, while that corresponding to the unmodified siRNA**23** duplex was not observed. Thus, the biaryl-modified siRNA**24** is more stable in PBS containing bovine serum than the unmodified siRNA**23**.

Inhibition of HCV Replication. The genome of hepatitis C virus (HCV) is encoded in an approximately 9.6 kb single-stranded RNA. Previously, we have shown that HCV replication is efficiently suppressed by siRNA**38** carrying a benzene-phosphate backbone at its 3′-overhang region (*22*). To assess the efficacy of biaryl-modified siRNAs, we compared the HCV replication-suppressing abilities of modified siRNAs with those of unmodified siRNAs. HCV replication is efficiently suppressed by siRNA targeted to an internal ribosome entry site (IRES) region (*30*), which was chosen as the target for this study. siRNA**38**, **39**, **40**, and **41** contain **B** or $\mathbf{B}^{\mathbf{n}}$ at the 5′ or 3′ ends of sense and antisense strands. siRNA**42** carries 4 mismatched bases in its sequence.

Figure 6 shows the results. The modified siRNAs, **38**−**41**, exhibited dose-dependent inhibition of HCV replication. They almost completely suppressed HCV replication at a concentration of 1 nM, while the replication ratio of siRNA**42**, which contained the mismatched bases, was 75% at the same concentration (Figure 6a). The siRNAs exerted no cytotoxic effect at 9 nM (Figure 6b). Thus, it was found that the modified siRNAs **38**−**41** suppressed HCV replication in a sequence-specific manner. At 0.11 nM, siRNA**39**, which carries the naphthalene type of biaryl unit, $\mathbf{B}^{\mathbf{n}}$, at the 5′ and 3′ ends of sense and antisense strands, was the most potent. Thus, $\mathbf{B}^{\mathbf{n}}$ modification also effectively improves the silencing activity of siRNAs targeting HCV.

In conclusion, we have demonstrated the synthesis of siRNAs modified with biaryl units. It was found that incorporation of the naphthalene biaryl unit, $\mathbf{B}^{\mathbf{n}}$, at the 5′ and 3′ ends of sense and antisense strands of siRNA improves silencing activity and nuclease resistance. Further, it was revealed that the modified siRNA suppressed HCV replication more efficiently than unmodified siRNA. Thus, the $\mathbf{B}^{\mathbf{n}}$ modification may hold promise as a method for improvement of the silencing activity and nuclease-resistance of siRNAs. Recently, it has been reported that lipophilic conjugates of oligonucleotides stimulate nonspecific immune response (*31*). The effects of the biaryl modifications of siRNAs on immune response are now under investigation.

EXPERIMENTAL SECTION

General Remarks. The NMR spectra were recorded at 400 MHz (^{1}H) and 100 MHz (^{13}C) and were reported in ppm downfield from tetramethylsilane. The coupling constants (J) are expressed in Hertz. Thin-layer chromatography was carried out on Merck coated plates 60F_{254}. Silica gel column chromatography was carried out on Wakogel C-300.

1-[3,5-Bis(hydroxymethyl)phenyl]benzene (2). A solution of 3,5-bis(*tert*-butyldimethylsilyloxymethyl)phenylboronic acid (1.00 g, 2.44 mmol) (*21*) in THF/H_2O (5:1, 12 mL) was added to a solution of 1-iodobenzene (0.50 g, 2.44 mmol) and $PdCl_2$(dppf)·CH_2Cl_2 (dppf is 1,1′-bis(diphenylphosphanyl)ferrocene) (0.089 g, 0.122 mmol) in THF/H_2O (5:1, 12 mL). 2 M NaOH (3.66 mL) was added to the mixture, and the whole was stirred at 65 °C for 24 h. The reaction mixture was filtered through Celite pad. The eluant was partitioned between EtOAc and H_2O. The

organic layer was washed with aqueous $NaHCO_3$ (saturated) and brine, dried (Na_2SO_4), and concentrated. The residue was dissolved in THF (12.2 mL). TBAF (1 M in THF, 7.3 mL) was added to the solution, and the mixture was stirred at room temperature for 2 h. The solvent was evaporated in vacuo, and the resulting residue was purified by column chromatography (SiO_2, 2% MeOH in $CHCl_3$) to give **2** (0.486 g, 93%): ^1H NMR ($CDCl_3$) δ 7.61−7.34 (m, 8H), 4.77 (s, 4H), 1.84 (s, 2H). ^{13}C NMR (DMSO-d_6) δ 133.9, 133.2, 132.9, 120.3, 118.8, 118.5, 116.0, 116.0, 55.7. Anal. Calcd for $C_{14}H_{14}O_2$: C, 78.48; H, 6.59. Found: C, 78.29; H, 6.46.

*1-[3-(4,4′-Dimethoxytrityloxymethyl)-5-(hydroxymethyl)phenyl]benzene (**10**).* A mixture of **2** (0.48 g, 2.24 mmol) and DMTrCl (0.76 g, 2.24 mmol) in pyridine (11 mL) was stirred at room temperature for 4 h. The mixture was partitioned between EtOAc and aqueous $NaHCO_3$ (saturated). The organic layer was washed with brine, dried (Na_2SO_4), and concentrated. The residue was purified by column chromatography (SiO_2, 15−45% EtOAc in hexane) to give **10** (0.601 g, 52%): ^1H NMR ($CDCl_3$) δ 7.61−7.21 (m, 17H), 6.87−6.83 (m, 4H), 4.77 (d, 2H, J = 5.6), 4.25 (s, 2H), 3.79 (m, 6H). ^{13}C NMR ($CDCl_3$) δ 158.5, 145.0, 141.5, 141.4, 141.0, 140.2, 136.2, 130.1, 128.7, 128.2, 127.8, 127.3, 127.2, 126.7, 125.1, 124.6, 124.5, 113.1, 86.5, 65.6, 65.4, 60.4, 55.2. Anal. Calcd for $C_{35}H_{34}O_5 \cdot H_2O$: C, 78.63; H, 6.41. Found: C, 78.64; H, 6.16.

*1-[3-[[(2-Cyanoethoxy)(N,N-diisopropylamino)phosphanyl]-oxymethyl]-5-(4,4′-dimethoxytrityloxymethyl)phenyl]benzene (**11**).* A mixture of **10** (0.42 g, 0.82 mmol), *N,N*-diisopropylethylamine (0.71 mL, 4.10 mmol), and chloro(2-cyanoethoxy)(*N,N*-diisopropylamino)phosphane (0.39 mL, 1.64 mmol) in THF (8 mL) was stirred at room temperature for 1 h. The mixture was partitioned between $CHCl_3$ and aqueous $NaHCO_3$ (saturated). The organic layer was washed with brine, dried (Na_2SO_4), and concentrated. The residue was purified by column chromatography (a neutralized SiO_2, EtOAc) to give **11** (0.52 g, 88%): ^{31}P NMR ($CDCl_3$) δ 149.0.

*1-[3,5-Bis(hydroxymethyl)phenyl]phenanthrene (**4**).* A solution of **7** in THF/H_2O (5:1, 12 mL) was added to a solution of 9-iodophenanthrene (0.74 g, 2.44 mmol) and $PdCl_2$(dppf)·CH_2Cl_2 (0.089 g, 0.122 mmol) in THF/H_2O (5:1, 12 mL). 2 M NaOH (3.66 mL) was added to the mixture, and the whole was stirred at 65 °C for 24 h. The reaction mixture was filtered through a Celite pad. The eluant was partitioned between EtOAc and H_2O. The organic layer was washed with aqueous $NaHCO_3$ (saturated) and brine, dried (Na_2SO_4), and concentrated. The residue was dissolved in THF (12.2 mL). TBAF (1 M in THF, 7.3 mL) was added to the solution, and the mixture was stirred at room temperature for 2 h. The solvent was evaporated in vacuo, and the resulting residue was purified by column chromatography (SiO_2, 2% MeOH in $CHCl_3$) to give **4** (0.47 g, 60%): ^1H NMR ($CDCl_3$) δ 8.76 (dd, 2H, J = 8.0 and 21.2), 7.89−7.87 (m, 2H), 7.70−7.48 (m, 8H), 4.82 (s, 4H), 1.80 (s, 2H). ^{13}C NMR ($CDCl_3$) δ 141.3, 140.9, 138.4, 131.4, 130.9, 130.5, 129.8, 128.5, 127.6, 127.3, 126.7, 126.6, 126.5, 126.4, 126.3, 124.4, 122.8, 122.4, 64.5. Anal. Calcd for $C_{22}H_{18}O_2 \cdot 1/5H_2O$: C, 83.10; H, 5.83. Found: C, 83.14; H, 5.86.

*1-[3-(4,4′-Dimethoxytrityloxymethyl)-5-(hydroxymethyl)phenyl]phenanthrene (**15**).* A mixture of **4** (0.46 g, 1.46 mmol) and DMTrCl (0.50 g, 1.46 mmol) in pyridine (7 mL) was stirred at room temperature for 3 h. The mixture was partitioned between EtOAc and aqueous $NaHCO_3$ (saturated). The organic layer was washed with brine, dried (Na_2SO_4), and concentrated. The residue was purified by column chromatography (SiO_2, 15−45% EtOAc in hexane) to give **15** (0.55 g, 61%): ^1H NMR ($CDCl_3$) δ 8.76 (dd, 2H, J = 8.0 and 22.0), 7.96−7.89 (m, 2H), 7.70−7.19 (m, 17H), 6.84−6.81 (m, 4H), 4.81 (s, 2H), 4.29 (s, 2H), 3.78 (m, 6H). ^{13}C NMR ($CDCl_3$) δ 158.4, 145.0, 141.0, 139.8, 138.5, 136.2, 131.5, 131.0, 130.6, 130.1, 129.9, 128.6, 128.2, 128.1, 127.8, 127.5, 127.4, 126.9, 126.8, 126.7, 126.6, 126.5, 126.4, 124.7, 122.9, 122.5, 113.1, 86.5, 65.6, 65.4, 55.2. Anal. Calcd for $C_{43}H_{36}O_4 \cdot 7/10H_2O$: C, 82.06; H, 5.99. Found: C, 82.04; H, 6.18.

*1-[3-[[(2-Cyanoethoxy)(N,N-diisopropylamino)phosphanyl]oxymethyl]-5-(4,4′-dimethoxytrityloxymethyl)phenyl]phenanthrene (**16**).* A mixture of **15** (0.35 g, 0.56 mmol), *N,N*-diisopropylethylamine (0.49 mL, 2.80 mmol), and chloro(2-cyanoethoxy)(*N,N*-diisopropylamino)phosphane (0.26 mL, 1.12 mmol) in THF (7 mL) was stirred at room temperature for 1 h. The mixture was partitioned between $CHCl_3$ and aqueous $NaHCO_3$ (saturated). The organic layer was washed with brine, dried (Na_2SO_4), and concentrated. The residue was purified by column chromatography (a neutralized SiO_2, EtOAc) to give **16** (0.34 g, 74%): ^{31}P NMR ($CDCl_3$) δ 149.0.

Solid Support Synthesis. A mixture of **10** (0.26 g, 0.50 mmol), succinic anhydride (0.15 g, 1.49 mmol), and DMAP (12 mg, 0.10 mmol) in pyridine (5 mL) was stirred at room temperature. After 24 h, the solution was partitioned between $CHCl_3$ and H_2O, and the organic layer was washed with H_2O and brine. The separated organic phase was dried (Na_2SO_4) and concentrated to give a succinate. Aminopropyl controlled pore glass (1.03 g, 0.12 mmol) was added to a solution of the succinate and EDCI (95 mg, 0.50 mmol) in DMF (12 mL), and the mixture was kept for 48 h at room temperature. After the resin was washed with pyridine, a capping solution (15 mL, 0.1 M DMAP in pyridine/Ac_2O = 9:1, v/v) was added and the whole mixture was kept for 24 h at room temperature. The resin was washed with MeOH and acetone, and dried in vacuo. The amount of loaded compound **10** to solid support was 49 μmol/g from calculation of released dimethoxytrityl cation by a solution of 70% $HClO_4$/EtOH (3:2, v/v). In a similar manner, solid support with **15** was obtained in 45 μmol/g loading amount.

RNA Synthesis. Synthesis was carried out with a DNA/RNA synthesizer by phosphoramidite method. Deprotection of bases and phosphates was performed in concentrated NH_4OH/EtOH (3:1, v/v) at room temperature for 12 h. 2′-TBDMS groups were removed by 1.0 M tetrabutylammonium fluoride (TBAF, Aldrich) in THF at room temperature for 12 h. The reaction was quenched with 0.1 M TEAA buffer (pH 7.0) and desalted on a Sep-Pak C18 cartridge. Deprotected ONs were purified by 20% PAGE containing 7 M urea to give the highly purified **ON45** (23), **ON46** (21), **ON47** (27), **ON48** (35), **ON49** (28), **ON50** (36), **ON51** (24), **ON52** (17), **ON53** (20), **ON54** (45), **ON57** (12), **ON58** (31), **ON59** (16), **ON60** (19), **ON63** (30), **ON64** (25), **ON65** (11), **ON66** (23), **ON69** (26), **ON70** (28), **ON71** (13), **ON74** (38), **ON75** (38), **ON76** (16), **ON77** (24), **ON78** (17), **ON79** (26). The yields are indicated in parentheses as OD units at 260 nm starting from 1.0 μmol scale. Extinction coefficients of the ONs were calculated from those of mononucleotides and dinucleotides according to the nearest-neighbor approximation method (*32*).

MALDI-TOF/MS Analysis of RNAs. Spectra were obtained with a time-of-flight mass spectrometer. **ON45**: calculated mass, 6443.9; observed mass, 6449.2. **ON46**: calculated mass, 6753.0; observed mass, 6751.8. **ON47**: calculated mass, 6543.9; observed mass, 6547.9. **ON48**: calculated mass, 6853.0; observed mass, 6853.2. **ON49**: calculated mass, 6644.0; observed mass, 6646.4. **ON50**: calculated mass, 6953.1; observed mass, 6951.0. **ON51**: calculated mass, 6696.0; observed mass, 6693.1. **ON52**: calculated mass, 7005.1; observed mass, 7004.8. **ON53**: calculated mass, 7067.0; observed mass, 7065.5. **ON54**: calculated mass, 7011.0; observed mass, 7007.9. **ON57**: calculated mass, 6859.2; observed mass, 6852.0. **ON58**: calculated mass, 6909.0; observed mass, 6902.4. **ON59**: calculated mass, 7008.3; observed mass, 7004.9. **ON60**: calculated mass, 7058.4; observed

mass, 7052.4. ON**63**: calculated mass, 6641.9; observed mass, 6645.5. ON**64**: calculated mass, 6688.0; observed mass, 6685.9. ON**65**: calculated mass, 6814.0; observed mass, 6820.1. ON**66**: calculated mass, 6522.9; observed mass, 6526.2. ON**69**: calculated mass, 6745.9; observed mass, 6746.1. ON**70**: calculated mass, 6568.9; observed mass, 6565.5. ON**71**: calculated mass, 6695.0; observed mass, 6696.0. ON**74**: calculated mass, 6739.9; observed mass, 6739.0. ON**75**: calculated mass, 6802.9; observed mass, 6801.4. ON**76**: calculated mass, 7066.0; observed mass, 7061.8. ON**77**: calculated mass, 6929.0; observed mass, 6933.2. ON**78**: calculated mass, 7066.0; observed mass, 7067.1. ON**79**: calculated mass, 6929.0; observed mass, 6931.6.

Thermal Denaturation Study. Each solution containing each siRNA (3 μM) in a buffer composed of 10 mM Na_2HPO_4/NaH_2PO_4 (pH 7.0) and 100 mM NaCl was heated at 95 °C for 3 min, then cooled gradually to an appropriate temperature, and used for the thermal denaturation studies. Thermally induced transitions of each mixture were monitored at 260 nm with a spectrophotometer.

Dual-Luciferase Assay. HeLa cells were grown at 37 °C in a humidified atmosphere of 5% CO_2 in air in Minimum Essential Medium (MEM) (Invitrogen) supplemented with 10% fetal bovine serum (FBS). Twenty-four hours before transfection, HeLa cells (4×10^4/mL) were transferred to 96-well plates (100 μL per well). They were transfected, using TransFast (Promega), according to instructions for transfection of adherent cell lines. Cells in each well were transfected with a solution (35 μL) of 20 ng of psiCHECK-2 vector (Promega), the indicated amounts of siRNAs, and 0.3 μg of TransFast in Opti-MEM I Reduced-Serum Medium (Invitrogen), and incubated at 37 °C. Transfection without siRNA was used as a control. After 1 h, MEM (100 μL) containing 10% FBS and antibiotics was added to each well, and the whole was further incubated at 37 °C. After 24 h, cell extracts were prepared in Passive Lysis Buffer (Promega). Activities of firefly and *Renilla* luciferases in cell lysates were determined with a dual-luciferase assay system (Promega) according to a manufacturer's protocol. The results were confirmed by at least three independent transfection experiments with two cultures each and are expressed as the average from four experiments as mean ± SD.

Partial Hydrolysis of ONs with Snake Venom Phosphodiesterase. Each ON (300 pmol) labeled with fluorescein at the 5′-end was incubated with snake venom phosphodiesterase (3 ng) in a buffer containing 37.5 mM Tris-HCl (pH 7.0) and 7.5 mM $MgCl_2$ (total 100 μL) at 37 °C. At appropriate periods, aliquots (5 μL) of the reaction mixture were separated and added to a solution of 9 M urea (15 μL). The mixtures were analyzed by electrophoresis on 20% polyacrylamide gel containing 7 M urea. The labeled ON in the gel was visualized by a Typhoon system (Amersham Biosciences).

Stability of siRNAs in the PBS Containing Bovine Serum. Each siRNA (600 pmol) labeled with fluorescein at the 5′-end of a sense strand was incubated in PBS (300 μL) containing 40% bovine serum at 37 °C. At appropriate periods, aliquots (5 μL) of the reaction mixture were separated and added to a loading solution (15 μL), and then the whole was immediately frozen in dry ice. The mixtures were analyzed by electrophoresis on 20% polyacrylamide gel under nondenaturing conditions. The labeled siRNA in the gel was visualized by a Typhoon system (Amersham Biosciences).

Subgenomic HCV Replicon Cells. Subgenomic HCV replicon cells (R6FLR-N) were conditional expression system of the HCV-nonstructure region and luciferase gene. These cells were cultured in DMEM-GlutaMAX High glucose (GIBCO) supplemented with 10% FBS, 1 unit penicillin (GIBCO), 100 μg/mL streptomycin (GIBCO), and 500 μg/mL G418 (GIBCO).

Transfection and Evaluation of Virus Replication. The subgenomic HCV replicon cells (R6FLR-N) were transfected with the siRNAs by reverse transfection. The cells were plated in 96-well plate (Falcon) at a density of 4×10^3 cells/well. Each siRNA (100 aM − 1 nM) was transfected to the cells using Lipofectamine RNAiMAX (Invitrogen) and Opti-MEM (GIBCO-BRL). The cells were incubated for 72 h after being transfected with siRNAs. HCV replication was evaluated by luminescence in a Mithras LB940 (Berthold Technologies, Wildbad, Germany) using Bright-Glo Luciferase Assay System (Promega) according to the manufacturer's protocol.

Cell Viability. In order to evaluate cytotoxic effects of the siRNAs, cell viabilities were measured by metabolic conversion of 2-(2-methoxy-4-nitrophenyl)-3-(4-nitrophenyl)-5-(2,4-disulfophenyl)-2*H*-tetrazolium, monosodium salt (WST-8) using a Cell Counting Kit-8 (Dojindo, Kumamoto, Japan) according to the manufactuer's protocol.

ACKNOWLEDGMENT

This study was supported in part by a Grant-in-Aid from Precursory Research for Embryonic Science and Technology (PRESTO) of Japan Science and Technology (JST) and a Grant-in-Aid for Scientific Research (C) from Japan Society for the Promotion of Science (JSPS) to Y.U. We are also grateful to Dr. Y. Kitamura (Gifu University) for providing technical assistance.

LITERATURE CITED

(1) Fire, A., Xu, S., Montgomery, M. K., Kostas, S. A., Driver, S. E., and Mello, C. C. (1998) Potent and specific genetic interference by double-stranded RNA in *Caenorhabditis elegans*. *Nature 391*, 806–811.

(2) Elbashir, S. M., Harborth, J., Lendeckel, W., Yalcin, A., Weber, K., and Tuschl, T. (2001) Duplexes of 21-nucleotide RNAs mediate RNA interference in cultured mammalian cells. *Nature 411*, 494–498.

(3) Elbashir, S. M., Lendeckel, W., and Tuschl, T. (2001) RNA interference is mediated by 21- and 22nucleotide RNAs. *Genes Dev. 15*, 188–200.

(4) Bumcrot, D., Manoharan, M., Koteliansky, V., and Sah, D. W. Y. (2006) RNAi therapeutics: a potential new class of pharmaceutical drugs. *Nat. Chem. Biol. 2*, 711–719.

(5) Behlke, M. A. (2006) Progress toward *in vivo* use of siRNAs. *Mol. Ther. 13*, 644–670.

(6) Kim, D. A., and Rossi, J. J. (2007) Strategies for silencing human disease using RNA interference. *Nat. Rev. Genet. 8*, 173–184.

(7) Schwarz, D. S., Hutvágner, G., Du, T., Xu, Z., Aronin, N., and Zamore, P. D. (2003) Asymmetry in the assembly of the RNAi enzyme complex. *Cell 115*, 199–208.

(8) Khvorova, A., Reynolds, A., and Jayasena, S. D. (2003) Functional siRNAs and miRNAsexhibit strand bias. *Cell 115*, 209–216.

(9) Tomari, Y., Matranga, C., Haley, B., Martinez, N., and Zamore, P. D. (2004) A protein sensor for siRNA asymmetry. *Science 306*, 1377–1380.

(10) Steiner, F. A., Hoogstrate, S. W., Okihara, K. L., Thijssen, K. L., Ketting, R. F., Plasterk, R. H. A., and Sijen, T. (2007) Structural features of small RNA precursors determine Argonaute loading in *Caenorhabditis elegans*. *Nat. Struct. Mol. Biol. 14*, 927–933.

(11) Mi, S., Cai, T., Hu, Y., Chen, Y., Hodges, E., Ni, F., Wu, L., Li, S., Zhou, H., Long, C., Chen, S., Hannon, G. J., and Qi, Y. (2008) Sorting of small RNAs into *Arabidopsis* Argonate complexes is directed by the 5′ terminal nucleotide. *Cell 133*, 116–127.

(12) Kawamata, T., Seitz, H., and Tomari, Y. (2009) Structural determinants of miRNAs for RISC loading and slicer-independent unwinding. *Nat. Struct. Mol. Biol. 16*, 953–960.
(13) Yoda, M., Kawamata, T., Paroo, Z., Ye, X., Iwasaki, S., Liu, Q., and Tomari, Y. (2010) ATP-dependent human RISC assembly pathways. *Nat. Struct. Mol. Biol. 16*, 17–23.
(14) Ghildiyal, M., Xu, J., Seitz, H., Weng, Z., and Zamore, P. D. (2010) Sorting of *Drosophila* small silencing RNAs partitions microRNA* strands into the RNA interference pathway. *RNA 16*, 43–56.
(15) Chen, P. Y., Weinmann, L., Gaidatzis, D., Pei, Y., Zavolan, M., Tuschl, T., and Meister, G. (2008) Strand-specific 5′-O-methylation of siRNA duplexes controls guide strand selection and targeting specificity. *RNA 14*, 263–274.
(16) Parker, J. S., Roe, S. M., and Barford, D. (2005) Structure insights into mRNA recognition from a PIWI domain-siRNA guide complex. *Nature 434*, 663–666.
(17) Ma, J.-B., Yuan, Y.-R., Meister, G., Pei, Y., Tuschl, T., and Patel, D. J. (2005) Structure basis for 5′-end-specific recognition of guide RNA by the *A. fulgidus* Piwi protein. *Nature 434*, 666–670.
(18) Wang, Y., Sheng, G., Juranek, S., Tuschl, T., and Patel, D. J. (2008) Structure of the guide-strand-containing argonaute silencing complex. *Nature 456*, 209–213.
(19) Wang, Y., Juranek, S., Li, H., Sheng, G., Tuschl, T., and Patel, D. J. (2008) Structure of an argonaute silencing complex with a seed-containing guide DNA and target RNA duplex. *Nature 456*, 921–926.
(20) Wang, Y., Juranek, S., Li, H., Sheng, G., Wardle, G. S., Tuschl, T., and Patel, D. J. (2010) Nucleation, propagation and cleavage of target RNAs in Ago silencing complexes. *Nature 461*, 754–761.
(21) Ueno, Y., Komatsuzaki, S., Takasu, K., Kawai, S., Kitamura, Y., and Kitade, Y. (2009) Synthesis and properties of oligonucleotides containing novel fluorescent biaryl units. *Eur. J. Org. Chem. 28*, 4763–4769.
(22) Ueno, Y., Watanabe, Y., Shibata, A., Yoshikawa, K., Takano, T., Kohara, M., and Kitade, Y. (2009) Synthesis of nuclease-resistant siRNAs possessing universal overhangs. *Bioorg. Med. Chem. 17*, 1974–1981.
(23) Lingel, A., Simon, B., Izaurralde, E., and Sattler, M. (2003) Structure and nucleic-acid binding of the *Drosophila* Argonaute 2 PAZ domain. *Nature 426*, 465–469.
(24) Yan, K. S., Yan, S., Farooq, A., Han, A., Zeng, L., and Zhou, M.-M. (2003) Structure and conserved RNA binding of the PAZ domain. *Nature 426*, 469–474.
(25) Song, J.-J., Liu, J., Tolia, N. H., Schneiderman, J., Smith, S. K., Martienssen, R. A., Hannon, G. J., and Joshua-Tor, L. (2003) The crystal structure of the Argonaute2 PAZ domain reveals an RNA binding motif in RNAi effector complexes. *Nat. Struct. Biol. 12*, 1026–1032.
(26) Ma, J.-B., Te, K., and Patel, D. J. (2004) Structure basis for overhang-specific small interfering RNA recognition by the PAZ domain. *Nature 429*, 318–322.
(27) Somoza, Á., Terrazas, M., and Eritja, R. (2010) Modified siRNAs for the study of the PAZ domain. *Chem. Commun. 46*, 4270–4272.
(28) Qiu, S., Adema, C. M., and Lane, T. (2005) A computational study of off-target effects of RNA interference. *Nucleic Acids. Res. 33*, 1834–1847.
(29) Jackson, A. L., Burchard, J., Schelter, J., Chau, B. N., Cleary, M., Lim, L., and Linsley, P. S. (2006) Widespread siRNA "off-target" transcript silencing mediated by seed region sequence complementarity. *RNA 12*, 1179–1187.
(30) Watanabe, T., Sudoh, M., Miyagishi, M., Akashi, H., Arai, M., Inoue, K., Taira, K., Yoshida, M., and Kohara, M. (2006) Intracellular-diced dsRNA has enhanced efficacy for silencing HCV RNA and overcomes variation in the viral genotype. *Gene Ther. 13*, 883–892.
(31) Uhlmann, E., Vollmer, J., and Krieg, A. M. (2010) Nucleic acid-lipophilic conjugates. U.S. Patent Appl. US 20100183639A1.
(32) Puglisi, J. D., and Tinoco, I., Jr. (1989) *In Methods in Enzymology*, Dahlberg, J. E., and Abelson, J. N., Eds.; pp 304–325, Vol 180, Academic Press, Inc., San Diego.

BC100301W

Arch Virol (2011) 156:295–304
DOI 10.1007/s00705-010-0859-x

ORIGINAL ARTICLE

Establishment of infectious HCV virion-producing cells with newly designed full-genome replicon RNA

Masaaki Arai · Hidenori Suzuki · Yoshimi Tobita · Asako Takagi · Koichi Okamoto · Atsunori Ohta · Masayuki Sudoh · Michinori Kohara

Received: 27 January 2010 / Accepted: 30 October 2010 / Published online: 19 January 2011

Abstract Hepatitis C virus (HCV) replicon systems enable in-depth analysis of the life cycle of HCV. However, the previously reported full-genome replicon system is unable to produce authentic virions. On the basis of these results, we constructed newly designed full-genomic replicon RNA, which is composed of the intact 5′-terminal-half RNA extending to the NS2 region flanked by an extra selection marker gene. Huh-7 cells harboring this full-genomic RNA proliferated well under G418 selection and secreted virion-like particles into the supernatant. These particles, which were round and 50 nm in diameter when analyzed by electron microscopy, had a buoyant density of 1.08 g/mL that shifted to 1.19 g/mL after NP-40 treatment; these figures match the putative densities of intact virions and nucleocapsids without envelope. The particles also showed infectivity in a colony-forming assay. This system may offer another option for investigating the life cycle of HCV.

M. Arai · A. Takagi
Pharmacology Research Laboratories I,
Mitsubishi Tanabe Pharma Corporation,
1000, Kamoshida-cho, Aoba-ku, Yokohama 227-0033, Japan

M. Arai · Y. Tobita · M. Kohara (✉)
Infectious Diseases Project, The Tokyo Metropolitan Institute of Medical Science, 1-6, Kamikitazawa, 2-chome, Setagaya-ku, Tokyo 156-8506, Japan
e-mail: kohara-mc@igakuken.or.jp

H. Suzuki
Laboratory for Electron Microscopy, Tokyo Metropolitan Institute of Medical Science, 1-6, Kamikitazawa, 2-chome, Setagaya-ku, Tokyo 156-8506, Japan

K. Okamoto · A. Ohta · M. Sudoh
Kamakura Research Laboratories, Chugai Pharmaceutical Co., Ltd., 200 Kajiwara, Kamakura, Kanagawa 247-8530, Japan

Introduction

Hepatitis C virus (HCV) is a major cause of chronic hepatitis, liver cirrhosis, and hepatocellular carcinoma. With over 170 million people currently infected [2], HCV is a growing public-health burden.

The life cycle of HCV has been difficult to study because cell culture and small animal models of HCV infection are not available. The recent development of HCV replicon systems has permitted the study of HCV translation and RNA replication in human hepatoma-derived Huh-7 cells in vitro [17]. However, these replicon systems cannot produce authentic virions because they lack the infection steps, and analysis of these infection steps is very important for understanding HCV pathogenesis.

Recently, some groups have successfully established in vitro infection systems [16, 21, 26, 28–30]. The strategies of these systems are basically the same as the ones used for transfection of Huh-7 cells or their derivatives with in vitro-generated HCV genome RNA [1]. The non-structural regions used in those studies were from the 2a genotype JFH (Japan Fulminant Hepatitis)-1 clone or the 1a genotype H77 clone. The former is known for its exceptionally vigorous amplification and broad permissiveness in cultured cells other than Huh-7 [3, 12, 13], while the latter shows only poor replication ability. Another group reported a newly established immortalized hepatocyte cell line that is susceptible to HCV infection, but only modest improvement was achieved [10]. There are also reports of a system using a full-genome replicon that has the entire coding region under the control of the internal ribosomal entry site of encephalomyocarditis virus, EMCV-IRES; however, this system also failed to show infectivity in the G418 selection assay [7, 20], and secretion of particles with the putative characteristics of HCV virions could not be confirmed [4].